Materials Today • Volume xxx, Number xx • xxxx 2021

ELSEVIER

Additive manufacturing and applications of nanomaterial-based sensors

Xiaoyu Sui [1,†], Julia R. Downing [2,†], Mark C. Hersam [2,3,4,5,*], Junhong Chen [6,7,*]

[1] Department of Mechanical Engineering, University of Wisconsin-Milwaukee, Milwaukee, WI 53201, USA
[2] Department of Materials Science and Engineering, Northwestern University, Evanston, IL 60208, USA
[3] Department of Chemistry, Northwestern University, Evanston, IL 60208, USA
[4] Department of Medicine, Northwestern University, Evanston, IL 60208, USA
[5] Department of Electrical and Computer Engineering, Northwestern University, Evanston, IL 60208, USA
[6] Pritzker School of Molecular Engineering, University of Chicago, Chicago, IL 60637, USA
[7] Chemical Sciences and Engineering Division, Physical Sciences and Engineering Directorate, Argonne National Laboratory, Lemont, IL 60439, USA

Nanoscale materials possess distinct physical and chemical attributes including size-dependent properties, quantum confinement, high surface-to-volume ratio, and superior catalytic activity. These unique qualities enable sensors with high sensitivity, robustness, and fast time response. As the emergence of the Internet of Things (IoT) demands increased production of sensors, it also provides an impetus for concentrated nanomaterial-based sensor research. Meanwhile, additive manufacturing (AM) of nanomaterial-based sensors is critical to bridge the gap between one-off, lab-scale fabrication and cost-effective, industrial-scale production with high reproducibility. By applying the design flexibility and cost savings of AM techniques, a new generation of nanomaterial-based sensing platforms can be integrated with IoT devices in the consumer space. Furthermore, emergent research in human–machine interfaces, food safety, and point-of-care diagnostics will be expedited by the development of sensors that can be printed with irregular form factors. In this Review, the relative strengths and weaknesses of printed sensor systems based on zero-, one-, and two-dimensional nanomaterials are discussed. In addition, sensors enabled by printable soft nanomaterials, heterostructures, and nanocomposites are surveyed due to their synergistic advantages for wearable healthcare monitoring and soft robotics. Finally, a roadmap for the next decade of research on this topic is provided.

Introduction

Sensors have revolutionized engineering systems with their ability to detect events or changes in the local environment, providing feedback to other electronic components. In the modern era, many different types of sensors (e.g., physical, chemical, and biological) are all converging on the nanoscale to simultaneously monitor multiple types of environmental stimuli [1–3]. Meanwhile, punctuated by the discovery of graphene[4], a plethora of nanoscale materials have emerged (Fig. 1) including zero-dimensional (0D) nanomaterials (e.g., fullerenes [5], metal nanoparticles [6], and quantum dots [7]), one-dimensional (1D) nanomaterials (e.g., nanotubes [8–10] and nanowires [11]), two-dimensional (2D) nanomaterials (e.g., graphene and graphene oxide [12], MoS_2 [13], black phosphorous [14], and MXenes [15]), and soft nanomaterials (e.g., nanostructured polymers [16,17]). The wide assortment of electronic, optical, and mechanical properties across these nanomaterial classes presents substantial opportunities for developing sensors with unprecedentedly high sensitivity, fast response, and robustness.

* Corresponding authors.
E-mail addresses: Hersam, M.C. (m-hersam@northwestern.edu), Chen, J. (junhongchen@uchicago.edu).
† These authors contributed equally.

 https://doi.org/10.1016/j.mattod.2021.02.001

Please cite this article in press as: X. Sui et al., Materials Today, (2021), https://doi.org/10.1016/j.mattod.2021.02.001

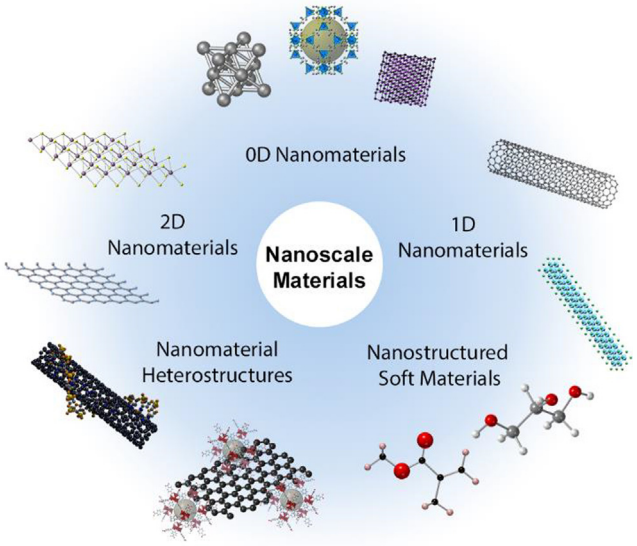

FIGURE 1

Overview of different classes of nanoscale materials used in printable sensing platforms.

The emergence of the Internet of Things (IoT) and the networking of smart objects have also significantly increased the demand for sensors and their implementation into both industrial applications and everyday life [18]. Conventional sensor technologies based on bulk semiconductors (e.g., silicon) are struggling to meet this emerging demand due to their rigid form factors since the intrinsically brittle nature of bulk inorganic semiconductors limits their deformation and conformal contact with irregular surfaces. Furthermore, the cost of bulk inorganic semiconductor devices increases proportionally to their footprint, limiting their cost-effectiveness to a few square millimeters [19]. Thus, it is imperative for researchers to advance alternative materials and manufacturing methods that enable fabrication of large-area sensing platforms.

Towards this end, material printing technologies are a subset of additive manufacturing (AM) that offer a solution for large-area, low-cost, high-throughput, and reproducible production of nanoelectronics and sensors on flexible substrates [19,20]. These attributes are ideal for key applications such as large-area flexible displays [21,22], low-cost disposable electronics for detection of hazardous chemicals [23,24], health monitoring [25,26], and wearable technologies [27,28]. Traditionally, AM techniques can be classified into two categories: contact and non-contact printing [29]. Contact printing entails bringing pre-patterned, inked templates or stencils into direct physical contact with the substrate to facilitate pattern transfer (e.g., screen printing [30], transfer printing [31,32], gravure printing [33], and flexographic printing [34]). In contrast, non-contact printing encompasses deposition techniques that eject functional nanomaterial inks onto a substrate from a standoff distance (e.g., inkjet printing (IJP) [35,36], electrohydrodynamic (e-jet) printing [37], aerosol jet printing (AJP) [38], spin/spray coating [39], and extrusion 3D printing (3DP) [40]. Meanwhile, versatile roll-to-roll printing (R2R) [41] is a burgeoning AM approach that combines attributes of multiple contact and non-contact printing processes to realize rapid prototyping. This suite of manufacturing strategies is summarized in Fig. 2.

Despite the rapid progress to date, researchers have not yet converged on a universal strategy that fully exploits the combined performance advantages of AM, sensing technologies, and nanomaterial properties. Existing reviews surrounding this topic are limited to only one or two of these areas at a time by focusing on lab-scale sensing technologies [3,36,43–48], AM without a sensor focus [49–53], one family of sensors (e.g., electromechanical sensors [54]), one subset of AM (e.g., non-contact printing only [55–58]), limited applications (e.g., healthcare [59,60], stretchable electronics [61–65]), a single subset of materials (e.g., 2D nanomaterials [42,66–68]), or dated examples [20] that do not indicate emerging IoT trends.

In this Review, the relative strengths and weaknesses of printed sensor systems based on zero-dimensional, one-dimensional, and two-dimensional nanomaterials are presented in terms of material-specific attributes that facilitate (1) superlative sensor performance and (2) suitability for AM. Beyond pristine, nanocrystalline structures, printed sensors based on hybrid materials (e.g., nanostructured soft materials, heterostructures, and nanocomposites are also discussed). Table 1 summarizes key contributions from nanomaterials and nanocomposites in AM sensors across prominent research areas from the past five years. We note that the different printing technologies within AM have very different physical requirements to achieve optimum deposition. Wu [53], Hu [42], and others have organized visual comparisons of printing resolution, throughput, and ink viscosity across many techniques, which can offer guidance during printing scheme selection and ink formulation. As AM matures, increasingly complex design capabilities coupled with decreasing fabrication costs will enable novel platforms that have previously been prohibitively expensive for consumer applications. Finally, a forward-looking perspective is provided at the end of this Review to encourage future research driven by high-throughput and statistically robust sensors enabled by printed nanomaterials.

Zero-dimensional nanomaterials

An arsenal of synthetic strategies enable control over structure–property relationships of zero-dimensional nanoparticles (NPs) [84]. Composition (e.g., pure metals, alloys, semiconducting metal oxides, and nonmetals), tunable size (1–100 nm), and shape (e.g., spherical, faceted, and branched) can all be tuned to realize different surface environments. These controllable features allow NPs to serve a range of important functions in sensing including (1) molecule immobilization and labeling, (2) reaction catalysis, (3) enhancement of electron transfer, and (4) transduction of environmental strain [85]. Additionally, their high surface-to-volume ratios enable efficient functionalization with a variety of ligands (e.g., DNA, enzymes) to enhance selectivity and sensitivity in biosensors. Thus, NPs are poised to enable emerging sensing platforms across multiple active research areas (Fig. 3). For large-area sensing arrays, AM offers the ability to deposit NP films with controllable porosity and control over signal-to-noise (S/N) ratio [84]. While AM schemes

Please cite this article in press as: X. Sui et al., Materials Today, (2021), https://doi.org/10.1016/j.mattod.2021.02.001

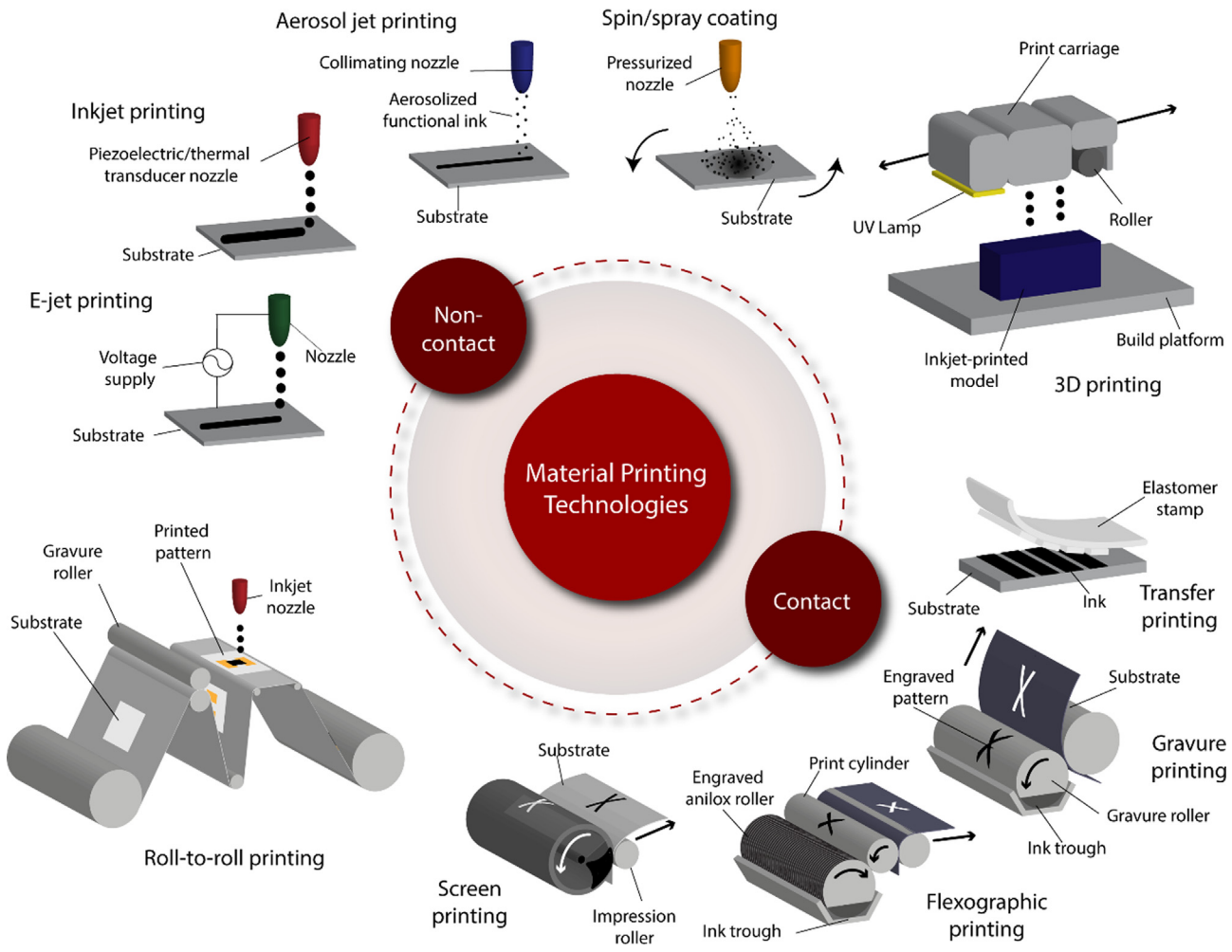

FIGURE 2

Additive manufacturing schemes for fabrication of nanomaterial-enabled sensors. These approaches are differentiated as non-contact methods, featuring impingement of the ink onto the substrate from a working distance, or contact-based methods, wherein the functional nanomaterial ink is deposited via mechanical interaction between the substrate and the desired pattern. Continuous manufacturing technologies such as roll-to-roll printing and 3D printing cannot be easily classified but incorporate both classes of printing modalities in sequential processes. Adapted with permission from [30,41,42]. Copyright © 2015 WILEY-VCH Verlag GmbH & Co. KGaA, Weinheim, © 2016 American Chemical Society, and © 2018 The Royal Society of Chemistry.

for fabricating NP-based sensors are still nascent, the last five years have seen significant progress towards new techniques to realize low-cost, NP-enabled solutions.

Metal nanoparticles

Many different metallic elements can be used to synthesize highly conductive nanoparticles, which are highly prevalent in some classes of physical sensors. These devices are responsive to touch, sound waves, and changes in temperature based on a change in the Ohmic resistance of the metal. Notably, silver (Ag) is the source material for the most common commercially produced NPs. AgNPs possess a high extinction coefficient, high electrical conductivity, strong Raman and fluorescence enhancement, and superior electrochemical activity [86]. The commercial availability of non-contact material inkjet printers and the reliable colloidal stability of conductive AgNP inks have readily enabled printable versions of conventional strain [87] and temperature sensors [88]. However, a lingering challenge is adapting these conventional geometries to corrosive environments without sacrificing device performance. Researchers have revamped traditional sensing geometries using digital printing techniques (e.g., IJP) to create precise, serpentine patterns of AgNPs for integrated heaters [17] and flexible resistance temperature detectors [89] on polymer substrates (e.g., polyimide (PI) and polyethylene terephthalate (PET)). This approach enables device operation at higher temperatures with a limited amount of material, significantly lowering intrinsic measurement error values in conventional devices [89].

Due to the high conductivity of silver, printable AgNP electrodes are also a workhorse for all-printed sensors that respond to human touch, particularly for large-area arrays (e.g., electronic skin or "e-skin"). For example, 25-pixel multifunctional sensor arrays using a conductive polymer sensing layer and AgNP electrodes have been created via transfer printing [94]. These printed electrodes can withstand several thousand bending cycles while operating at low voltages, indicating substantial promise for conformal lamination to the skin and other irregular surfaces for environmental sensing (e.g., ambient light detection) [95].

Please cite this article in press as: X. Sui et al., Materials Today, (2021), https://doi.org/10.1016/j.mattod.2021.02.001

TABLE 1

Overview of printed nanomaterial-based sensors including the most relevant performance figure of merit.

Application	Sensor Ability	Performance	Constituent Nanomaterial	Dimensionality	Printing Type	Ref.
Environmental Monitoring	Thermal mapping	Yield = 98 ± 0.8%, with uncertainty of 3.9 ± 2.9 K *(modified continuous-wave optically detected magnetic resonance)*	Nanodiamonds	0D	Transfer	[32]
	Food spoilage detection	Sensitivity = 225%, 46%, and 17% *(5 ppm ammonia NH_3, putrescine, and cadaverine, respectively)*	Nanostructured PAni	1D polymer	Inkjet	[69]
	Counterfeiting detection	Response time = 0.2–0.5 s to saturation *(EtOH)*	SiO_2 nanoparticles, colloidal photonic nanocrystals	0D	Inkjet	[70]
	Water quality detection	Low limit of detection = 10^2 bacteria mL^{-1} *(colorimetric assay, E. coli XL1)*	Au nanoparticles	0D	Inkjet	[71]
	Toxic gas identification	Sensitivity = 74.6%, with a response time of 12 s *(50 ppm NO_2 in air)*	Ag nanoparticles, Sulfonated rGO	0D/2D	Gravure	[72]
	Photodetectors	Responsivity = 164 mA W^{-1} *(visible and near-infrared wavelengths)*	Black phosphorous	2D	Inkjet	[14]
	Humidity detection	Linear detection range = 25–100% RH *(alternating current electroluminescent display)*	Graphene oxide, Nafion	2D/polymer	Screen	[73]
	Heavy metal detection	Low limit of detection = 0.07 ppb *(square-wave anodic stripping voltammetry, Pb^{2+})*	Graphene oxide, PDMS	2D/polymer	Screen	[74]
Biosensing	Protein and virus detection	Low limit of detection = 5 pg/mL *(Nonfaradaic electrochemical impedance spectroscopy, pp65-antigen of human cytomegalovirus)*	ZnO nanoparticles	0D	Flexo-graphic	[34]
	Fluorescence detection	Low limit of detection = 10^{-16} mol L^{-1} *(fluorescence analyte, R6G, and molecular fluorophore-based cocaine assays)*	Poly(StMMA-AA) nanospheres	0D	Inkjet	[75]
Health Monitoring	Immunosensing	Linear detection range = 0.2 – 50 ng/mL *(cyclic voltammetry, H. pylori)*	ZnO nano-tetrapods	0D	Screen	[76]
	Point-of-care diagnostics	Linear detection range = 1–50 × 10^{-9} M *(enzyme-linked immunosorbent assay, FAM/biotin reporters)*	PEG nanoparticles	0D polymer	3D	[77]
	Body acceleration and temperature	Multifunctional. Temperature sensitivity ~0.89%/°C Acceleration of ~20 m/s^2 detected in three directions.	Ag nanoparticles, Carbon nanotubes, PEDOT:PSS	0D/1D/polymer	Screen	[78]
Soft Robotics	Tactile sensing	Piezoelectric coefficient (d_{31}) of 18 pC N^{-1} *(impedance spectroscopy)*	$BaTiO_3$ nanoparticles, PVDF	0D/polymer	3D	[79]
	Acoustic sensing	Linear resistance change = $\varepsilon \leq 1\%$ and up to 50%	Ag nanoparticles, SBS	0D/polymer	3D	[80]
	Precise motion detection	Gauge factor = 2392.9 at 62% strain	Fullerenes, Ag nanowires, graphene oxide	0D/1D/2D	Screen	[81]
Human-Machine Interfaces	Touch screens	Linear detection range = 1–2 Hz *(short-circuit current)*	Carbon nanotubes	1D	Screen	[82]
	Electronic skin	Limit of detection = 28 Pa, with sensitivity of 0.5 kPa^{-1}	Reduced graphene oxide	2D	Transfer	[83]

Regardless of the target application, reproducible fabrication of AgNP electrodes makes them easy to integrate with multi-step fabrication schemes for achieving advanced device geometries.

Beyond tactile, acoustic, and thermal sensing, metal NPs are also effective in types of chemical sensors that rely on changes that are normally detected by "taste" or "sight" on the nanoscale. Reliable detection in biological environments is another grand challenge in which AgNP-enabled biosensors [90,96] exhibit fluorescent properties to reach extremely low detection limits and high sensitivity to biomolecules in bodily fluids. For example, microcontact printing techniques combined with surface-enhanced Raman scattering together enable selective sensing domains on branched-DNA-functionalized AgNP films, allowing for simultaneous sensing of multiple liver cancer biomarkers in serum down to the attomolar limit (Fig. 3**a**) [90]. The ability of screen-printed AgNPs to cross-link with enzymes via electropolymerization has also shown the broader utility of AgNP material properties for consumer-targeted biosensing platforms [88].

Other than silver, gold (Au) is the most common metal used to synthesize NPs for chemical-based sensing (e.g., in electrochemical and biosensors, lateral flow assays, colorimetric assays, and plasmonics). The intense, visible color of AuNPs and their facile conjugation with biological ligands offer a highly compatible environment for biomolecules in a manner that is also generally nontoxic to cells [86]. Conventional AM methods have been implemented to harness these properties in low-cost,

Please cite this article in press as: X. Sui et al., Materials Today, (2021), https://doi.org/10.1016/j.mattod.2021.02.001

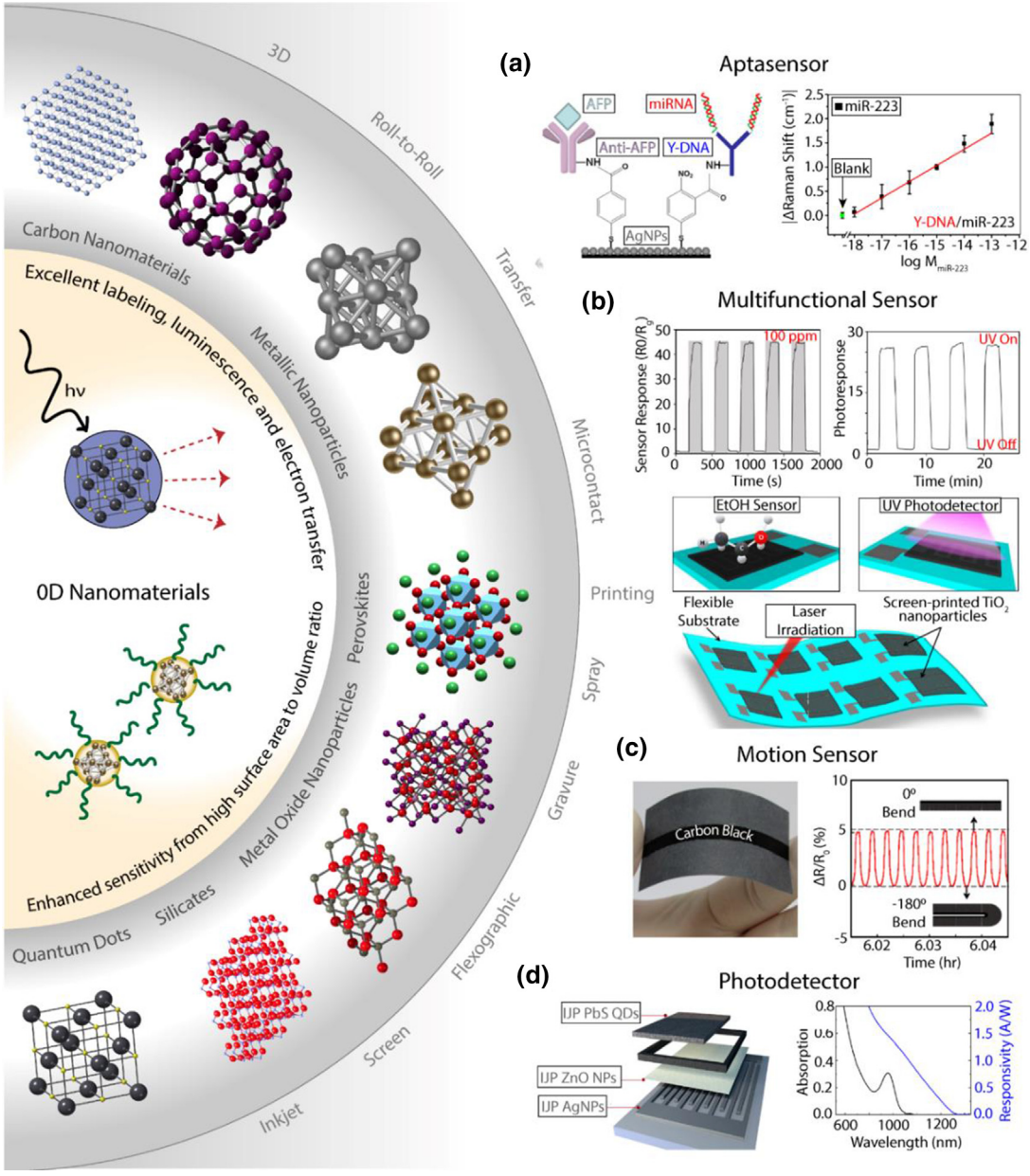

FIGURE 3

Tunable surface characteristics of 0D nanomaterials enable a broad range of printed sensing modalities. Nearly all types of crystalline matter have been synthesized into spheres 1–100 nm in diameter with tunable surface-to-volume ratios, offering customizable platforms for ligand functionalization, thin film fabrication, post-processing, and more [84]. The presence of a wide breadth of additive manufacturing techniques applied to nanoparticle inks in emergent literature also reflects the powerful customizability of this material platform. (a) DNA functionalization of microcontact-printed Ag nanoparticle thin films for attomolar detection of cancer biomarkers. Reproduced with permission from [90]. Copyright © 2018 American Chemical Society. (b) Screen-printed TiO_2 nanoparticles tuned by laser irradiation. Reproduced with permission from [91]. Copyright © 2019 American Chemical Society. (c) Fully-printed conductive carbon black nanostructures on paper for high-performance electronic, electrochemical, and wearable devices. Reproduced with permission from [92]. Copyright © 2017 American Chemical Society. (d) Inkjet-printed infrared photodetectors based on PbS nanocrystals with perovskite ligands. Reproduced with permission from [93]. Copyright © 2019 American Chemical Society.

field-based applications (e.g., inkjet-printed, paper-based drinking water test strips employing enzyme-functionalized AuNPs) [71]. Beyond IJP, more exotic manufacturing schemes are also emerging (e.g., printing self-propelled anti-pinning ink droplets [97] and layer-by-layer contact printing [98]) that exploit the ability of AuNPs to readily cross-link with polymer ligands, forming sizable sensing planes with minimal active material.

With these advantages in mind, materials-centric manufacturing engineering can be deployed to sensors based on metals that are even more reactive to chemical stimuli. Palladium (Pd) is extremely important for electrochemical applications due to its high electrocatalytic activity and affinity for hydrogen. IJP helps to lower the cost of PdNP sensors with its low-waste, on-demand deposition characteristics offering control over Pd oxidation. For example, IJP coupled with a two-step thermolysis process can successfully produce continuous, uniform Pd films from high-loading PdNP inks [99]. The resulting films exploit the differing oxidation states of PdNPs in the surface and bulk regions to

Please cite this article in press as: X. Sui et al., Materials Today, (2021), https://doi.org/10.1016/j.mattod.2021.02.001

detect minute ambient changes in the environment (e.g., pH). Similarly, Zn-based devices are plagued by uncontrollable surface oxidation, so evaporation–condensation-mediated laser printing [100] has been developed to rapidly print and sinter ZnNPs in confined dimensions while maintaining strong crystallinity. Representative resistive-type strain sensors perform on par with evaporated metal films but have the advantage of printability via R2R processing. Thus, future sensing paradigms utilizing metal NPs will rely on non-contact printing methods that limit exposure to oxygenated environments. Additionally, techniques combining contact printing with pulsed laser sintering of alloyed NPs (e.g., CuAu) are also promising [101].

Metal oxide nanoparticles

Semiconducting metal oxide (MO) materials can exhibit changes in electrical resistance in response to chemical stimuli, making their 0D forms ideal for chemiresistors [1,91]. Through chemical interactions such as covalent/hydrogen bonding or molecular binding, MO-NP sensors can "taste" or "smell" their target analyte's with high selectivity. However, several materials-centric challenges exist for MO-NP-based devices, including the need for high operating temperatures to achieve maximum performance, vulnerability to mechanical strain, and difficulty in processing the material into different shapes. While some printed MO-NP sensors perform well at room temperature [102], emerging printed MO-NP sensing platforms employ diverse fabrication schemes to circumnavigate these material challenges. Contact printing methods are more commonly deployed for MO-NP sensors than for their metal NP counterparts. Notably, multifunctional screen-printed TiO_2 sensors featuring properties tuned by laser irradiation [91] (Fig. 3**b**) have recently emerged, and the ability to tune MO properties in multi-step printing processes enables R2R printing of large-area sensors [103,104] using different types of MO-NPs.

Indeed, for MO-NP sensors the biggest manufacturing challenges are (1) large-area fabrication and (2) demanding form factors that introduce mechanical strain to the MO-NP film. In the arena of large-area scalable manufacturing, another high-throughput R2R production scheme for ZnO thin-film sensors enables scalable screening for human cytomegalovirus detection [34]. Towards achieving printed sensors with demanding form factors, manufacturing-scale non-contact printing methods are generally incompatible with nonplanar form factors, although ultrathin sensory coatings of In_2O_3 NPs have been developed [105]. Researchers may have to develop multi-step conformal printing and sintering schemes to meet this challenge. Finally, AM is highly attractive for select MO materials (e.g., refractory ceramics) that are difficult to shape by conventional machining or casting methods. 3DP is rushing to meet this need, enabling construction of sensory structures out of piezoelectric $BaTiO_3$ NPs via stereolithography [106]. These manufacturing strategies are highly attractive because they can achieve near-bulk material density (above 90%), thus maximizing materials-driven sensory performance.

Nonmetals

In chemical sensors, fullerenes (C_{60}) are electroactive carbon molecules that possess multiple redox states but are highly hydrophobic, thus presenting a challenge for ink formulation engineering in AM fabrication schemes [84]. However, NPs based on other carbon allotropes have shown promise in physical sensing applications such as nanocrystalline diamond [32,107]. Mass sensors designed using this extraordinary material outperform lithographically produced counterparts when fabricated using an office-grade inkjet printer, reaching detection limits of hundreds of zettagrams at a low cost [107]. A related physical application is thermal sensing, wherein spatial detection with nanometer resolution is critical for monitoring the heat distribution in high-density electronics [32]. Thus, low-cost and low-waste IJP can be a powerful tool for integration of otherwise expensive 0D nanomaterials into inexpensive physical sensors. Taking it one step further, amorphous carbon NPs have shown success in 3DP "touch" sensors; researchers have successfully fabricated strain sensors using a carbon black/cellulose acetate ink that can be deposited using a customized 3D inkjet printer [92] (Fig. 3**c**). Finally, to complete the picture of sensing physical stimuli, IJP is also useful for precise location of other sensitive nonmetal NPs, e.g., mesoporous SiO_2 photonic nanocrystals [108] and zeolite NPs [109] that respond to light.

Quantum dots

Enabling sensors that can "see" light, quantum dots (QDs) are 0D fluorescent semiconductor nanocrystals with dimensions in the 1–10 nm range that are highly relevant for photodetectors, biosensors, and optoelectronics. Lead sulfide (PbS) QDs are a central material platform for QD inks, owing to their strong absorption over a broad wavelength spectrum. However, a ligand exchange processing step is often needed to stabilize QDs in functional inks, posing significant challenges for large-area printing [84]. In the seminal demonstration of inkjet-printable PbS photodetectors, the complex ink formulation required perovskite-like ligands and a ternary solvent system to achieve stable printing [93] (Fig. 3**d**). For stretchable sensors, transfer printing is the incumbent approach, with stretchable PbS photodetectors successfully used for monitoring photoplethysmography signals [110]. In next-generation QD sensor systems, a critical bottleneck will be scalable synthesis of QDs to enable growth beyond batch-scale fabrication of biomedical electronic devices (e.g., by R2R printing).

To summarize, 0D nanomaterials offer (1) a wide variety of functional surface chemistries, (2) high surface-to-volume ratios that enable high sensor sensitivity, and (3) a breadth of commercially available material inks that offer a stable platform for AM process innovations. In the coming decades, researchers will have to focus on devising manufacturing processes that circumnavigate sensitive NP chemistries and enable non-planar device construction to realize large-area, conformal NP sensing schemes.

One-dimensional nanomaterials

One-dimensional (1D) nanomaterials are the extension of their 0D counterparts in one direction, with high aspect ratios and cross-sectional diameters less than 100 nm [111]. Their 1D geometry minimizes the number of grain boundaries in the material structure, lowering brittleness at the boundary areas while under

Please cite this article in press as: X. Sui et al., Materials Today, (2021), https://doi.org/10.1016/j.mattod.2021.02.001

strain. Along with their intrinsic mechanical elasticity, 1D nanomaterials also satisfy the key requirement for flexible electronics – namely, robustness to mechanical deformation. Finally, a 1D charge pathway confined to exposed atoms on the surface makes 1D nanomaterials highly sensitive to environmental perturbations. This endows 1D materials a distinct advantage for chemical sensing applications [112,113].

According to percolation theory, 1D materials with high aspect ratios also effectively lower the percolation threshold when forming films with conductive networks [114,115]. Hence, a network can be constructed economically via percolation junctions with minimal amounts of material. Furthermore, the 1D building blocks need not fully cover the conductive areas, leaving void spaces to accommodate mechanical deformation in flexible electronics. The permeable networks of 1D materials also enable high transparency and breathability, which are highly desirable in transparent electronics [116] and wearable sensor devices [82], respectively. These properties are extremely difficult to achieve synergistically from other types of nanomaterials, making 1D nanomaterials (e.g., carbon nanotubes, metal oxide, and perovskite nanowires) attractive in photoelectronic, chemical, mechanical, and wearable sensing devices fabricated by AM (Fig. 4).

Carbon nanotubes

Carbon nanotubes (CNTs) are comprised of one (single-walled, SWCNTs) or several (multi-walled, MWCNTs) concentric layers of graphene sheets rolled up into a cylindrical shape. MWCNTs are typically metallic, with a current-carrying capacity as high as 10^9 A cm^{-2} [117]. Meanwhile, SWCNTs can be either metallic or semiconducting depending on the nanotube chiral vector [118,119]. CNTs notably exhibit outstanding mechanical properties resulting from the sp^2-carbon hexagonal lattice and nanotube structure with fracture strengths exceeding 100 GPa [120].

Arc discharge techniques, pulsed laser deposition (PLD), and chemical vapor deposition (CVD) are three common synthesis methods of CNTs [19], and post-growth separation is usually required for nanotube purification [127]. In thin-film transistor (TFT) sensing devices, CNTs can be used to print both the highly conductive circuit components and the semiconducting sensing channels depending on their metallic or semiconducting character. Furthermore, printed CNT-based conductive electrodes take advantage of the excellent conductivity and high surface area of CNTs. For example, inkjet printing has yielded electrodes with sheet resistance values as low as 132 Ω/□ in electrochemical sensor systems [9,121].

To make use of the excellent semiconducting properties of CNTs, purified SWCNTs can be deposited with high resolution via AJP, forming TFT channels on flexible polyimide substrates. These channels show significant promise for flexible, transistor-enabled sensors, exhibiting a hysteresis-free I_{on}/I_{off} ratio of $\sim 6 \times 10^4$ and stable current modulation even after 1000 bending cycles [128]. When printed CNT networks are deposited on elastomeric substrates, stretchable strain sensors for motion detection have also exhibited controllable gauge factors up to 35.75 [129].

Additionally, the geometric design freedom of AM has led to further improvements in both multi-directional and stretchable aspects of CNT-based strain sensors. Multi-directional strain sensors can be realized by combining several individual devices printed in different directions [129]. To further enhance the stretchability of CNT-based devices, a free-standing serpentine pattern has been designed and screen printed for an additional degree of stretchability beyond the intrinsic stretchable CNT network (Fig. 4**a**) [121]. The resulting devices can withstand up to 500% strain while maintaining structural integrity and stable performance. Highly stretchable electrochemical sensors for ammonium and glucose detection, as well as stretchable biofuel cells and any combination thereof, can be constructed based on this printed CNT platform.

However, a major challenge for system-level integration of SWCNT devices is augmentation of self-powered sensors, where triboelectric nanogenerators have become one of the most promising target applications. When screen-printed CNT electrodes are sandwiched between two judiciously selected fabrics (e.g., nylon as substrate and silk as top layer), wearable systems such as a self-powered touch/gesture sensor become practical for human–machine interfacing (Fig. 4**b**) [82]. These innovative textile-based sensing platforms show excellent stability under mechanical deformation, even after washing. Such innovations make futuristic technologies such as clothing-integrated, smart controllers for IoT home appliances tractable.

To create CNT conductive networks on non-planar topographical surfaces, hydrogel-templated transfer printing is an emerging strategy for flexible tactile sensors [130]. Formulation of hydrogel inks often requires dispersants or surfactants, which must be removed after printing to avoid suppressed CNT conductivity. During this transfer printing process, the hydrogel template can simultaneously remove dispersants, thus eliminating the need for subsequent chemical/thermal removal. 3DP helps further extend CNT-based electronics to free-standing structures, such as CNT-based emitters, gas sensors, and radio frequency inductors (Fig. 4**c**) [131]. Highly conductive MWCNT microstructures with high material loading (~75 wt.%), spatial resolutions of a few micrometers, and conductivities ~2540 S m^{-1} can also be obtained by this method.

Finally, apart from the superior mechanical and electrical properties of CNTs, their near-infrared fluorescence can also be utilized for label-free, multiplexed nano-biosensor arrays fabricated by a microarray printer (Fig. 4**d**) [123]. This optical sensing platform enables real-time *in situ* monitoring of binding interactions between capture proteins and antibodies, which are governed by proximity quenching of the intrinsic fluorescence of SWCNTs by the analyte. Binding kinetics between the analyte and SWCNTs should be investigated in parallel to provide more insight about reversible and transient reactions. Despite many excellent properties of SWCNTs in optoelectronic, chemical, and mechanical aspects, further refinement of both controlled synthesis and post-synthesis separation remains of interest to address polydispersity issues (e.g., various chiral species with distinct properties) [132].

Metal/metal oxide nanowires

Metals and metal oxides are also promising sensing materials due to their high conductivities and rich electronic properties, respectively. One-dimensional nanostructures greatly boost the

Please cite this article in press as: X. Sui et al., Materials Today, (2021), https://doi.org/10.1016/j.mattod.2021.02.001

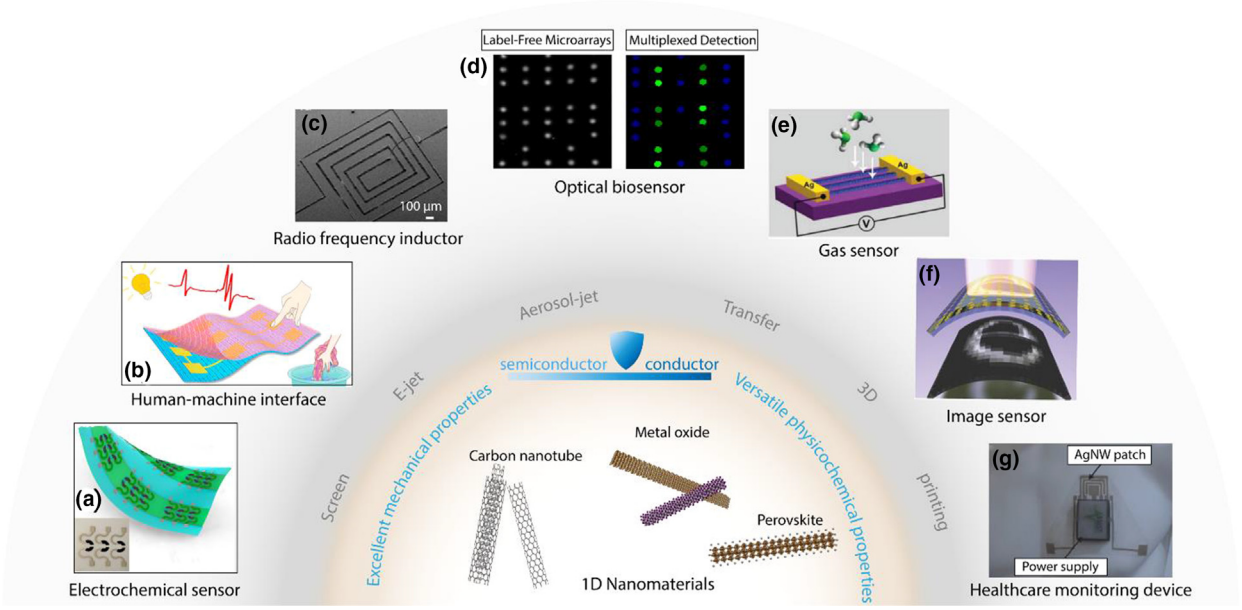

FIG. 4

Robust mechanical strength and diverse physicochemical properties of 1D nanomaterials are crucial for system-level, multifunctional sensing paradigms. (a) Highly stretchable, serpentine CNT-based electrochemical sensor. Reproduced with permission from [121]. Copyright © 2015 American Chemical Society. (b) Self-powered CNT-based touch/gesture sensing device for human–machine interfacing. Reproduced with permission from [82]. Copyright © 2018 American Chemical Society. (c) 3D-printed CNT radio frequency inductor. Reproduced with permission from [122]. Copyright © 2016 American Chemical Society. (d) Multiplexed, SWCNT-based optical biosensor. Reproduced with permission from [123]. Copyright © 2018 American Chemical Society.(e) E-jet printed polycrystalline Zn_2GeO_4 wire sensor for ultrasensitive detection of ammonia gas. Reproduced with permission from [124]. Copyright © 2018 WILEY-VCH Verlag GmbH & Co. KGaA, Weinheim. (f) Highly crystalline blade coated $CH_3NH_3PbI_3$ arrays as photodetectors with robust long-term stability. Reproduced with permission from [125]. Copyright © 2016 WILEY-VCH Verlag GmbH & Co. KGaA, Weinheim. (g) 1D nanomaterials enabling a multi-functional healthcare monitoring system. Reproduced with permission from [126]. Copyright © 2017 WILEY-VCH Verlag GmbH & Co. KGaA, Weinheim.

surface-to-volume ratio and provide access to other relevant features of these materials. For example, solvent-assisted transfer printing enables highly-fidelity reproduction of sub-20 nm metallic patterns comprised of Au-, Al-, Cu-, Ag-, Co-, Cr- and Pd-nanowires (NWs) onto diverse receiver surfaces [133]. A simple polydimethylsiloxane (PDMS) gel pad can be employed as the solvent-emitting transfer medium to weaken the interfacial friction energy, releasing the adhesive film during transfer printing. This method is efficient and versatile, enabling gas sensors composed of 20-nm-wide PdNW arrays for fast (8 s) and highly sensitive detection of H_2 (concentration: 0.1%) [133].

Instead of AM with pre-synthesized NWs, e-jet printing through near-field electrospinning can also be employed to deposit a mixed solution containing metal precursors and sacrificial polymers (e.g., polyvinylpyrrolidone) into continuous, digitally controlled, and arbitrarily long NW patterns. After sintering, morphology-preserved MO-NWs with diameters down to 100 nm have been obtained [124,131]. This method has proven to be highly general as various pristine (e.g., ZnO, SnO_2, WO_3, and In_2O_3), doped (e.g., nanoparticle-doped ZnO), and alloyed MO-NWs (e.g., InZnO and Zn_2GeO_4-NWs) with enhanced electrical characteristics have been prepared. For example, AM-enabled ZnO-NW gas sensors exhibit higher responsivities to NO_2 compared to a lithographic ZnO thin film control. Similarly prepared polycrystalline Zn_2GeO_4 -NW sensors enable ultrasensitive detection to ammonia gas (~600% response upon 100 ppm) owing to the highly active defects in the grain boundaries, which facilitate ammonia gas adsorption and improved electronic transport for catalytic reactions (Fig. 4**e**). Besides gas sensors, field-effect transistors (FETs) fully composed of MO-NWs are also viable with high carrier mobility ($\mu \sim 17.67\ cm^2\ V^{-1}s^{-1}$) and high transmittance being especially promising for FET-based sensing architectures.

Perovskite nanowires

Inorganic–organic hybrid perovskite materials are attractive for optoelectronic devices, such as solar cells and photodetectors, due to their high optical absorption coefficients and long carrier lifetimes. However, the excessive number of grain boundaries in common polycrystalline perovskite thin films hinder performance in practical device operation. To ameliorate this issue, highly aligned and uniform single-crystalline perovskite microwire arrays have been fabricated by a simple, low-cost blade coating method. For example, as-coated highly crystalline $CH_3NH_3PbI_3$ arrays with minimal grain boundaries enable photodetectors with robust long-term stability (>50 days in air) in addition to high responsivity (13.57 A W^{-1}) and specific detectivity (5.25×10^{12} Jones) (Fig. 4**f**) [125,134]. The combined success of these single-crystalline perovskite microwire arrays prepared by blade coating and polycrystalline Zn_2GeO_4 wire arrays prepared by e-jet printing confirm that AM offers nanowire synthesis routes with crystal structure tunability that can

Please cite this article in press as: X. Sui et al., Materials Today, (2021), https://doi.org/10.1016/j.mattod.2021.02.001

be tailored to specific sensing applications.

Overall, the urgent need for personalized health care monitoring continues to stimulate the development of wearable multifunctional sensing systems based on 1D nanomaterials for real-time data acquisition and preventive care (Fig. 4**g**). 1D nanomaterials are critical for such applications due to their superlative mechanical strength and versatile physicochemical properties. CNTs can be fabricated into flexible strain gauges for motion monitoring, tactile/pressure sensors for electrocardiograms, and temperature sensors; meanwhile ZnO-NWs are suitable for light sensors [95] and optoelectronic applications. With regards to scale-up, R2R printing has the potential for mass production of flexible sensors based on nanowire properties at a low cost, which will reduce device variability and enable systems-level integration.

Two-dimensional nanomaterials

Two-dimensional (2D) nanomaterials can be isolated from bulk solids comprised of atomically thin layers held together in the out-of-plane direction by van der Waals forces. Top-down exfoliation processes yield atomically thin and few-layer nanosheets composed of materials ranging from elemental carbon to transition metal dichalcogenides. These 2D nanomaterials are characterized by diverse electronic character and a large, active surface area that is ideal for sensor applications. Individual sheets can be hundreds of nanometers across in the lateral dimension, while possessing thicknesses at the nanometer or even atomic scale. 2D nanomaterial synthesis is at varying levels of development; some methods are approaching the manufacturing scale, although scalability can be limited by ambient reactivity or incorporation of toxic, high-boiling-point solvents [68]. Some of the most prominent applications for 2D nanomaterials are advanced electronics and optoelectronics [67], including TFTs and photodetectors, respectively (Fig. 5). Key challenges in the manufacturing space for these materials are mechanical adhesion, optimized percolation of 2D nanosheets, and functionalization with other nanomaterials [67].

Graphene

Graphene was the first two-dimensional nanomaterial to be discovered, and its mechanical robustness and high electrical conductivity have since enabled a range of printable inks that span the continuum of additive manufacturing technologies and sensing applications. It is impossible to capture the full breadth of prior research pertaining to additively manufactured graphene devices and graphene-based sensors in this Review. Instead, we have curated forward-looking examples confined to the past five years and emphasize future opportunities for overlap between material-specific properties and AM (e.g., multifunctional sensors and all-printed sensors, final perspective Section). Entire Reviews have been dedicated to 2D-printed graphene [66] and graphene-based electronic sensors [139] should readers want to further explore graphene-centric research in these areas.

Key properties of the graphene nanosheets for optimized device performance vary widely, and graphene's robustness and high processability are constantly enabling discontinuous advancements in both printed chemical and resistive-type sensor technologies. Chemical sensors require pristine graphene with tunable carrier concentration, while electrical conductivity is the most important characteristic for TFTs, strain sensors, and conductive electrodes [42]. Meanwhile, high surface area and defect density are the key attributes for graphene nanosheets destined for electrochemical functionalization. For biosensing and electroanalysis, graphene can be modified with different biomolecular markers and complementary 0D and 1D nanomaterials [66].

Graphene-based sensors are already well-established in non-contact AM schemes, with IJP being the predominant fabrication method for applications ranging from humidity sensing [72] to multifunctional temperature/tactile sensors for e-skin applications [140]. For ultrathin devices (e.g., supercapacitors for self-powered sensors), other layer-by-layer non-contact printing techniques such as spray printing are attractive [141]. Furthermore, the mechanical robustness and ambient stability of graphene have enabled researchers to begin pushing past the resolution limits of IJP for biosensing applications. Notably, inkjet massless lithography has been explored to achieve line widths of printed graphene as small as 20 microns, resulting in devices that are able to detect organophosphates at the 3 nM limit of detection [142]. More recently, AJP has been used to fabricate biosensors targeting similar analytes [143].

Meanwhile, new contact printing schemes are being developed for wearable graphene sensors. Key challenges for manufacturing-scale integration of these devices include (1) high-quality contact formation for graphene electrodes in multifunctional device arrays and (2) interfacial adhesion control between polymeric substrates and percolating graphene films. Researchers have tackled these challenges by transfer printing multifunctional device arrays, resulting in high-quality temperature and tremor sensors on epidermal patch platforms designed for Parkinson's disease [144] and diabetes patients [145] (Fig. 5**a**). Indeed, serpentine graphene patterns coupled with printed solid-state reference electrodes (e.g., Ag/AgCl) will continue to be pivotal for healthcare monitoring. Beyond the healthcare field, contact-based AM schemes like screen printing are less common, but slowly emerging in wireless radio-frequency identification for broad IoT applications due to advances in formulation engineering with "green" components [146]. Finally, researchers are leveraging the geometric design freedom of 3DP to create ultralight sensing structures from graphene without sacrificing conductivity [147].

Graphene oxide and reduced graphene oxide

The electronic character of graphitic sensing elements (e.g., conducting, or semiconducting) varies based on the synthetic approach for graphene, notably top–down exfoliation from bulk graphite or reduction of insulating graphene oxide (GO) produced via the Hummers method. While GO does not boast current modulation as high as other 2D nanomaterial semiconductors, its highly defective structure, room-temperature stability, and hydrophilic nature are useful for chemical sensing. Its oxygen-containing functional groups (–O–, –OH and –COOH) are highly permeable to water, allowing for broad sensing capabilities once activated. These advantages have been showcased in screen-printed electroluminescent displays functionalized with GO, enabling smartphone-compatible humidity sensors that rely on proton-hopping to

Please cite this article in press as: X. Sui et al., Materials Today, (2021), https://doi.org/10.1016/j.mattod.2021.02.001

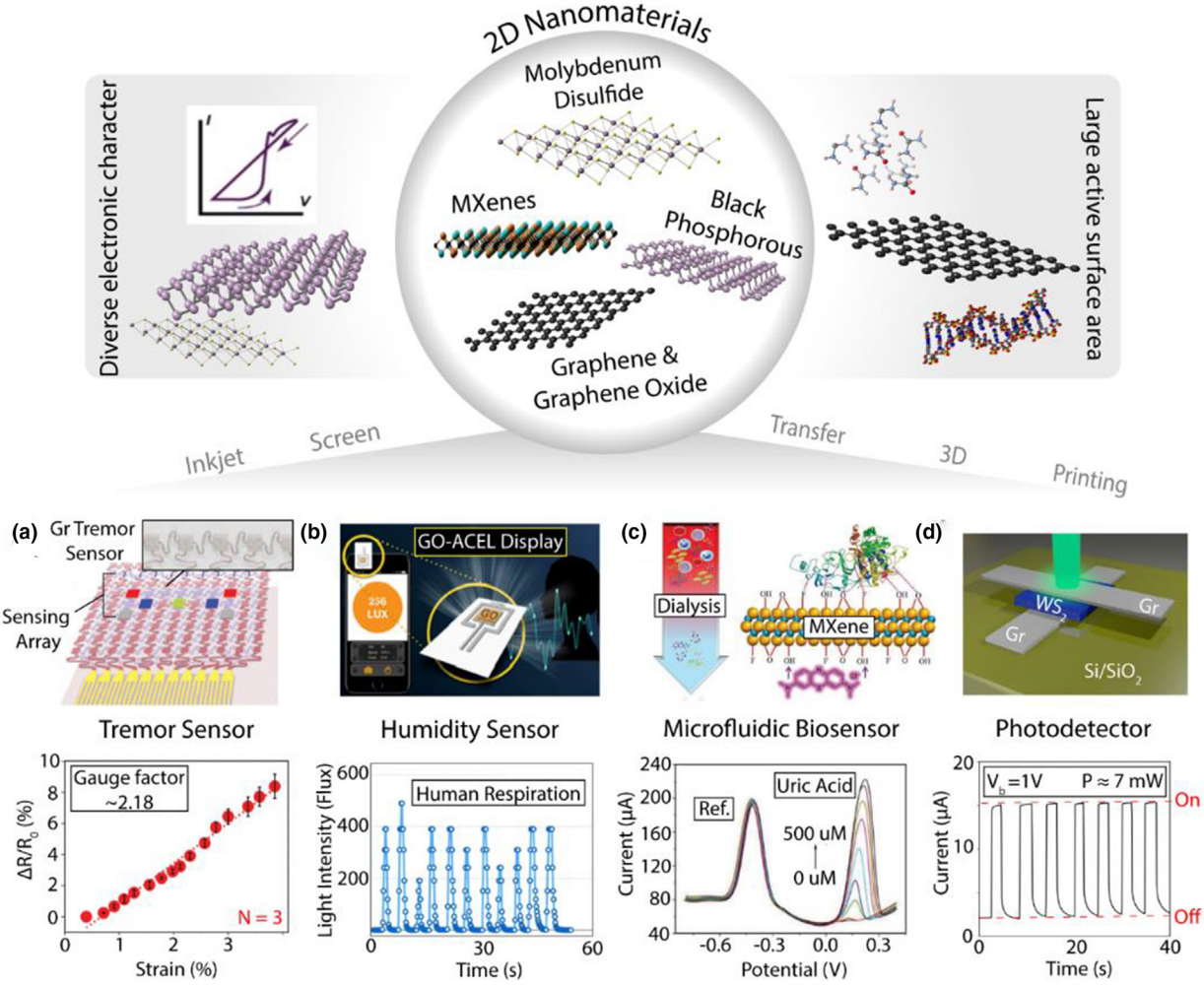

FIG. 5

Versatile sensing applications enabled by inkjet-printed and screen-printed 2D nanomaterials with diverse electronic and electrochemical characteristics. Top: semiconducting behavior of black phosphorus. Reproduced with permission from [135]. Copyright © 2015 American Chemical Society. (a) Graphene-based electrochemical device with thermoresponsive microneedles for diabetes monitoring and therapy. Reproduced with permission from [136]. Copyright © 2016 Springer Nature. (b) Screen-printable, graphene-oxide-based vapor sensors for respiratory monitoring. Reproduced with permission from [73]. Copyright © 2018 American Chemical Society. (c) MXene-enabled electrochemical microfluidic biosensor for continuous monitoring of whole blood. Reproduced with permission from [137]. Copyright © 2018 WILEY-VCH Verlag GmbH & Co. KGaA, Weinheim. (d) All-inkjet-printed graphene/WS_2/graphene photodetector. Reproduced with permission from [138]. Copyright © 2017 Springer Nature.

increase conductance in the material [73] (Fig. 5**b**). While IJP of GO/rGO was first demonstrated in NO_2 gas sensing schemes over a decade ago [12,72,148], contact-printing-based AM schemes are still evolving to tailor GO for printable patient diagnostics using DNA-functionalized [149] and R2R printed devices [150]. Furthermore, dopamine biosensors can be realized via inkjet reduction [146] by depositing a reducing agent directly onto a GO substrate, reaching conductivity values as high as 8000 S m^{-1} while avoiding nozzle clogging phenomena characteristic of colloidal IJP. Achieving high conductivity with rGO while preserving chemically functionalized defects is critical for maintaining specificity in environmental sensing.

MXenes

A highly conductive alternative to graphene has emerged in MXenes, which are nanosheets exfoliated from bulk MAX stochiometric alloys via wet etching and other chemical methods. While their harsh synthesis has limited the realization of scalable production of MXenes, screen-printed sensors have been realized recently for microfluidic biosensing applications (Fig. 5**c**) [137] and self-powered force sensors [151]. These examples highlight some of the unique advantages of MXenes for sensing; their accordion-like, multi-layer architectures [137] are ideal for continuous detection. Their high electrical conductivity also enables tactile sensors with strong responsivity. Finally, tunable arrangements and terminations of the transition metal layers can be used to control the material's band structure for optoelectronic sensing platforms.

Transition metal dichalcogenides

2D transition metal dichalcogenides (TMDCs) are layered crystals with MX_2 stoichiometry, where M is a transition metal atom and X is a chalcogen atom. TMDCs, unlike graphene and MXenes, offer a direct electronic bandgap and strong spin–orbit coupling

Please cite this article in press as: X. Sui et al., Materials Today, (2021), https://doi.org/10.1016/j.mattod.2021.02.001

to printed sensor systems; they are semiconductors in their thermodynamically favorable 2H-phases [152].

Molybdenum disulfide (MoS_2) is the most ubiquitous 2D TMDC in printed sensors, boasting high photoresponsivity, high FET mobility (>200 $cm^2 V^{-1} s^{-1}$), and superior switching characteristics ($I_{on}/I_{off} \sim 10^8$) [13], all of which make it highly suitable for optoelectronic applications. Still, AM of MoS_2 to produce large-area sensing arrays is relatively rare and confined to digital printing. IJP of MoS_2 often requires caustic, complex solvent ensembles, and printed devices have been unable to match the mobility or photoresponse of single-flake MoS_2 sensors. However, formulation engineering is relaxing challenges arising from printing pristine MoS_2. For example, photodetectors [153] can be constructed using a mixture of double-phased MoS_2 (both 1T and 2H) in conjunction with MoO_3 using IJP. Higher responsivity in these devices compared to other liquid-phase-exfoliated MoS_2 photodetectors can be attributed to enhanced photoelectron generation by using both MoS_2/MoO_3, as well as high electrical conductivity and efficient charge transfer from metallic 1T MoS_2. These strategies will enable a wider range of applications for MoS_2 in rugged optoelectronic sensors.

Other promising TMDCs for printed nanomaterial-based sensors include tungsten disulfide (WS_2), which has been inkjet-printed alongside graphene to fabricate high-performance photodetectors [138]. Molybdenum diselenide ($MoSe_2$) [154] and tungsten diselenide (WSe_2) [155] have led to lithographically produced gas sensors, notably extending the reach of TMDCs beyond photodetectors, which may be graduated to AM via ink formulation engineering in the future.

Monoelemental 2D nanomaterials

Black phosphorous (BP), or phosphorene, is another 2D nanomaterial with a thickness-dependent band gap and high FET mobility. However, its sensitivity to ambient conditions presents challenges for AM-enabled sensors. Some of these challenges have been overcome using anhydrous organic solvents [156] and deoxygenated aqueous solutions [157] to enable stable BP dispersions. In addition, encapsulation [158] and chemical passivation [159] schemes have been developed to preserve the electronic properties of BP in ambient conditions. When properly handled, BP FETs have been achieved that show high selectivity for NO_2 gas sensing [160]. In addition, scalable fabrication of photodetectors based on BP is possible with careful optimization of IJP [14]. For highly sensitive 2D nanomaterial semiconductors, researchers should focus on omitting binders to constrain ink deposition to Marangoni flow conditions and select solvent chemistries that rapidly facilitate drying to avoid oxidation and loss of photoresponsivity [42].

At the time this article was written, practical examples of sensors utilizing other monoelemental 2D nanomaterials such as silicene [161,162] and borophene [163,164] were limited to first-principles calculations. These studies, while impressive, are still too early in their genesis to discuss rapid deployment of additive manufacturing of sensors using these materials.

2D nanomaterial heterostructures

The concurrent use of multiple 2D nanomaterials can further enhance the sensitivity of emergent optoelectronic devices and optical sensors [42]. However, fabrication of heterostructure devices is intrinsically challenging due to the need to have clean and well-defined interfaces between the disparate 2D nanosheets. IJP, with its ability to maintain precise alignment between multiple printing steps, has been the most widely studied platform for printed 2D heterostructure devices. For example, all-printed graphene/WS_2/graphene photodetectors fabricated using water-based biocompatible inks boast photoresponsivities higher than 1 mA W^{-1} (Fig. 5**d**) [138]. Other successful approaches have relied on polymer-mediated exfoliation and subsequent annealing processes to achieve graphene/MoS_2/-graphene photodetectors [165] with an additional order of magnitude of improvement in photoresponsivity. Contact-based, multi-material printing techniques are still being developed for 2D nanomaterial inks and will better enable other types of all-printed sensors based entirely on 2D nanomaterials.

To review, 2D nanomaterials are distinguished by high surface areas, unique topology, and ample defect sites for functionalization. However, more work is necessary to close the gap between lab-scale AM demonstration of 2D nanomaterial-based sensors and manufacturing-scale production of devices. Key innovations that are required include: (1) binder engineering in inkjet-printable inks to realize non-Newtonian, shear-thinning behavior; (2) development of conformal contact printing techniques for 2D nanomaterials; (3) large-scale studies of simultaneous biomarker sensing capabilities of nanosheets over extended periods; and (4) identifying facile, "green" synthesis schemes for more exotic 2D nanomaterials such as MXenes.

Nanostructured soft materials

Soft materials here refers to polymers with flexible molecular backbones, which were considered to be electrically insulating until the discovery of highly conductive, iodine-doped polyacetylene [166]. The excellent processability of polymers, which has been traditionally exploited in restrictive manufacturing techniques such as molding, is highly compatible with AM techniques for customizable sensor architectures. Other key material properties such as high flexibility, stretchability, and material compatibility have recently facilitated their emergence in flexible and wearable sensing systems (Fig. 6).

Organic conductors and semiconductors

Poly(3,4-ethylenedioxythiophene):poly(styrene sulfonate) (PEDOT:PSS) is a ubiquitous conductive polymer with high conductivity, processability, and stability. Electrical conductivity as high as 4380 S cm^{-1} has been achieved from H_2SO_4-treated PEDOT:PSS [167], and the thermoelectric and piezoresistive qualities of PEDOT:PSS can also be utilized for simultaneous temperature and pressure monitoring by quantitatively transducing temperature–pressure stimuli into distinct signals [168]. This type of structure is well-represented in wearable "e-fingers" with spatially resolved pressure and temperature sensitivity, which have been fabricated via IJP of PEDOT:PSS onto textiles (Fig. 6**a**). To enhance the stretchability of PEDOT:PSS required for wearable and large-area electronic technologies, multiple strategies have been developed including blending with plasticizers or other

Please cite this article in press as: X. Sui et al., Materials Today, (2021), https://doi.org/10.1016/j.mattod.2021.02.001

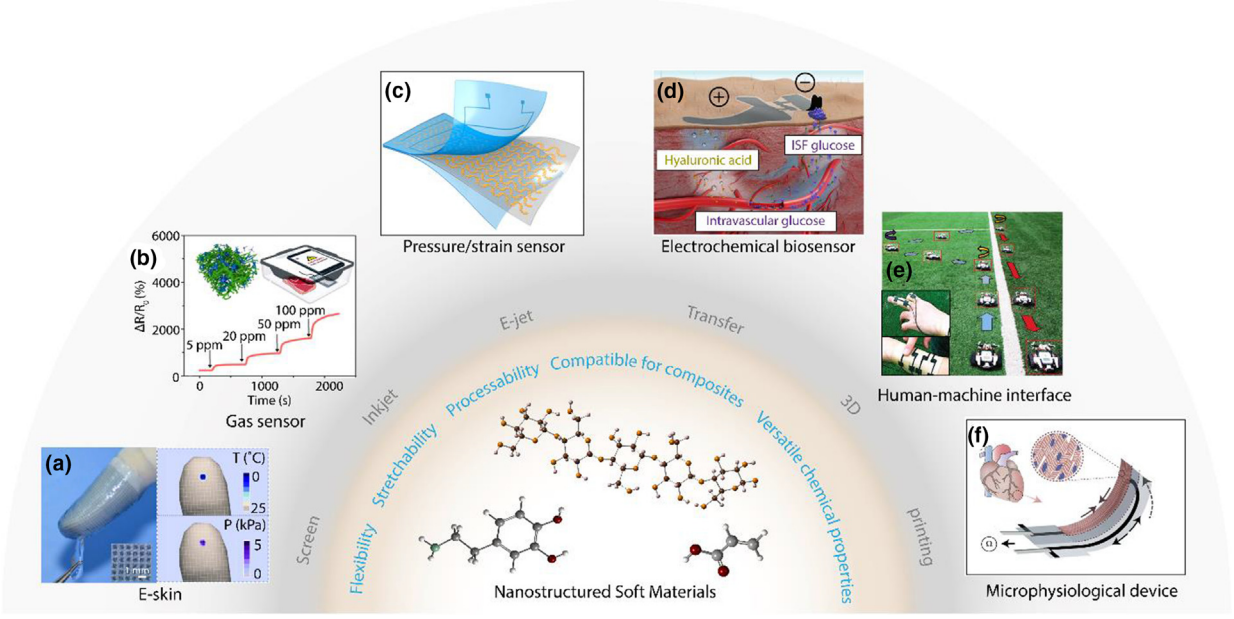

FIG. 6

Processability and flexibility of nanostructured polymer sensing platforms allow for scalable manufacturing and lamination onto irregular surfaces. (a) PEDOT:PSS-based e-skin array. Reproduced with permission from [168]. Copyright © 2015 Springer Nature. (b) Modified PAni network for gas sensing. Reproduced with permission from [69]. Copyright © 2018 American Chemical Society. (c) PVDF-enabled, self-powered mechanical sensor. Reproduced with permission from [70]. Copyright © 2017 Elsevier Ltd. (d) PMMA/PI thin films supporting noninvasive blood glucose biosensors. Reproduced with permission from [170]. Copyright © 2017 The Authors, AAAS under a CC BY-NC license. (e) Porous PDMS/MWCNT nanocomposites used as a human–machine interface. Reproduced with permission from [26]. Copyright © 2014 WILEY-VCH Verlag GmbH & Co. KGaA, Weinheim. (f) Polymer-based microphysiological monitoring system. Reproduced with permission from [171]. Copyright © 2016 Springer Nature.

polymers, embedding in stretchable matrices, and forming hydrogels and fibers [169].

Polyaniline (PAni) is another conductive polymer with high biocompatibility and outstanding biosensing performance. Polymerization of monomers can occur either before or after printing, and porous foam-like networks of PAni provide abundant active sites for chemical sensing pathways. Additionally, PAni hydrogels are an effective interfacial material between electrodes and biological species in electrochemical sensors, offering large surface areas for enzyme immobilization and a high-quality electrical interface. Exploiting these properties, IJP of PAni has been used to fabricate amperometric, multiplexed biosensors with high sensitivity and selective detection of lactate, glucose, and triglycerides in real time [172]. Iron(III) p-toluene sulfonate hexahydrate-doped PAni networks are also sensitive to amine gases, showing a significant resistance change in the presence of ammonia and biogenic amines (e.g., $\Delta R/R_0$ of 225%, 46%, and 17% upon exposure to 5 ppm of NH_3, putrescine, and cadaverine, respectively). The resistance change of doped, IJP-fabricated PAni is sufficiently high for switching in near-field communication systems designed for food spoilage detection (Fig. 6**b**) [69]. The morphology of PAni can be further controlled by using an enzyme-like nanofibrous hydrogel as both the scaffold and catalyst, resulting in a hybrid microstructure [43].

Furthermore, ion-conductive hydrogels are emerging materials that use charged ions instead of electrons for charge transport. A polyacrylamide–poly(ethylene glycol) ionic hydrogel prepared by co-cross-linking two photo-sensitive hydrogels with distinct mechanical properties illustrates the design freedom of this approach [173]. These hydrogels can be printed using stereolithography (SLA), imparting tunable mechanical properties to the resulting nanostructure. Another hydrogel based on a physically and chemically cross-linked, polypyrrole-grafted chitosan (PPy-DCh) and poly(acrylic acid) (PAA) network is similarly able to combine the electrical conductivity of PPy with the ionic conductivity from Fe^{3+} ions [174]. In addition, the highly reversible ionic interactions between the Fe^{3+} ions and carboxylic groups of PAA lead to rapid self-healing (e.g., 100% mechanical recovery in 2 min and 90% electrical recovery in 30 s). The hydrogel is highly stretchable up to 15-fold and can be patterned by 3DP into capacitive or resistive sensors for high-fidelity motion detection.

Compared to conductive polymers, relatively few reports have employed semiconducting polymers for printed sensors due to the limited number of candidate materials. A key exception is the mass manufacturing of n-type polymeric semiconductor films based on poly[N,N′-bis(2-octyldodecyl)-naphthalene-1,4,5,8-bis(dicarboximide)-2,6-diyl]-alt-5,5′-(2,2′-bithiophene) (P(NDI2-OD-T2)) via room-temperature, wired-bar coating [175]. This coating method can direct the self-assembled polymer chains into large-area, sub-monolayer nanostructured films. The highly ordered and elongated microstructure results in FET mobilities up to 6.4 $cm^2\ V^{-1}\ s^{-1}$ and an operational frequency exceeding 3 MHz, which is among the highest values for polymeric n-type semiconductors. The intrinsically flexible nature and excellent electrical properties of P(NDI2OD-T2) nanostructures show high potential for wearable and distributed sensors.

Please cite this article in press as: X. Sui et al., Materials Today, (2021), https://doi.org/10.1016/j.mattod.2021.02.001

Other polymer-based systems

Cellulose is the most abundant biopolymer in the world with a periodic structure and abundant, reactive hydroxyl groups along the polymer chains. By taking advantage of these regularly arranged hydroxyl groups, cellulose derivatives with high solubility, processability, and mechanical strength can be prepared through simple chemical reactions. For example, hydroxypropyl cellulose (HPC) forms a helical liquid-crystalline phase, enabling colorimetric shifts from Bragg reflections [176]. The cellulosic nanostructure is highly sensitive to external stimuli and can be used in responsive photonic sensors. A scalable R2R printing process can produce mechano-chromic HPC laminates at the meter-scale, enabling recording of a 2D pressure distribution with smart-phone integration [177]. Luminogens can also be covalently immobilized onto the hydroxyl groups to introduce color responsivity to biogenic amines [178]. Owing to its high solubility and processability, the material can be processed into a diverse array of structures.

For detection in solution, low analyte concentration is still a major challenge for sensor systems. In this context, AM can be used to enrich sparse analytes onto nanostructured polymer sensors. For example, in a photonic crystal (PC) microchip, hydrophilic monodispersed poly(styrene-methyl methacrylate-acrylic acid) spheres were printed by IJP onto a hydrophobic PDMS substrate, concentrating fluorescent analytes onto their hydrophilic surfaces to improve detection of analytes and fluorophore-based assays down to a LOD of 10^{-16} mol L^{-1} [75].

Furthermore, self-powered mechanical sensing systems are being enabled by piezoelectric polymers. One such material, poly(vinylidene fluoride) (PVDF), can be patterned into self-similar serpentine nano/microfibers via e-jet printing (Fig. 6**c**). Patterned PVDF exhibits excellent piezoelectric performance, high stretchability (>300%), low LOD (0.2 mg), and outstanding durability (>1400 times at stain of 150%) [70]. The strong electric fields and mechanical stretching forces during e-jet printing align the dipoles in the PVDF fibers, contributing to the strong piezoelectricity [179]. Meanwhile, the hierarchical serpentine structures are formed by controlling the "whipping/buckling" instability of e-jet printing, resulting in high stretchability [70]. This alignment effect on printed materials is prominent in extrusion-type printing methods, including e-jet printing and 3D extrusion printing.

Beyond using pristine polymers with intrinsic sensing capabilities, polymer compatibility with other material systems enables advanced sensing nanocomposites. As matrix materials, polymers can impart mechanical support and enable integration of complex multi-component material systems. For example, polymethyl methacrylate (PMMA)/polyimide (PI) thin films have been employed as the substrate for a noninvasive blood glucose biosensor system, ensuring its flexible and intimate contact with the skin (Fig. 6**d**) [170]. In other cases, ink formulation engineering (e.g., via reverse micelle solutions) can be leveraged with conductive nanomaterials to create highly sensitive porous nanostructures (Fig. 6**e**) [26]. Finally, emergent AM schemes such as 3DP are well-suited to exploit the processability of polymers, as will be discussed further in the next section. 3DP is particularly valuable in tissue engineering, where polymers with piezoresistive, high-conductance, and biocompatible features can be implemented in strain gauge sensors in artificial organ systems (Fig. 6**f**) [171].

Nanocomposites and heterostructures

For the purposes of this Review, the terms "heterostructure" and "nanocomposite" will be distinctly defined. Here, sensing devices with multiple nanosized material components that are deposited separately but brought into contact to function together in the final device are termed "heterostructures". In contrast, "nanocomposites" are fabricated with multimaterial functional inks, resulting in a homogeneous microstructure throughout. Some composites are binary, having just two components (i.e., a 0D/1D/2D nanomaterial and polymer matrix) while others are polynary, having multiple nanomaterial components with or without a polymer matrix material. During ink formulation, solvent engineering in the nanocomposite can be employed to improve processability (e.g., mitigating nozzle clogging in extrusion or jetting processes). This section will focus on the synergistic aspects of the constituent materials in nanocomposites and heterostructures.

Binary nanomaterial heterostructures

Devices based on mixed-dimensional heterostructures [180,181] (e.g., 0D/1D, 0D/2D, and 1D/2D) have been realized with a range of AM techniques. Well-studied materials systems such as Ag/Au/Si NPs (0D), CNTs/AgNWs (1D), and graphene (2D) drive innovation with their tunable properties, mechanical strength, and high electrical conductivity, respectively. Ultrathin material layers are critical for flexible heterostructures, but high performance in electro-tactile systems have been difficult to achieve due to mechanical mismatch and rigid components. Multi-dimensional, transparent nanomaterials (e.g., graphene and AgNWs) reduce rigidity and improve S/N ratios when printed onto deformable polymer substrates [182]. Other combinations of printed elastomers and silicon nanomembranes/nanoribbons enable wearable biosensors that can be resorbed by the body (when printed on biodegradable elastomers). These so-called "transient electronics" are consumed via simple hydrolysis reactions, and exhibit reliable performance in strain, pH, and electrophysiological sensing [183].

From a manufacturing perspective, however, a key challenge for multifunctional sensors is precise placement of components of different dimensionalities without compromising intricate device geometries and sensitivity. Here, high-precision transfer printing is a valuable tool, but its scalability is hindered by lithography-based steps prior to printing. However, recent analytical modeling efforts and finite element modeling are enabling transfer printing to realize system-level wearable bioelectronics for clinical settings [185]. Digital printing techniques such as IJP and AJP further enable combined heterostructure and nanocomposite approaches. Using more advanced optoelectronic materials like QDs [186] and self-healing nanostructured polymers [187], high-performing sensors can be realized. Combining multiple species of QDs in a polymer matrix enables IJP of photodetectors with a 10^3 improvement over a single QD/graphene device by capitalizing on the properties of the

Please cite this article in press as: X. Sui et al., Materials Today, (2021), https://doi.org/10.1016/j.mattod.2021.02.001

nanocomposite sensitizer in a high mobility heterostructure [186]. Meanwhile, IJP of multi-polymer, self-healable dielectric layers leads to unusually high capacitance to conformal environmental sensors [187].

Binary, ternary and polynary nanocomposites

In a classical strain sensor, high sensitivity relies on materials that must deform substantially under minute strain. Meanwhile, highly stretchable sensors rely on high mechanical integrity under large loads. Meeting these competing demands is extremely challenging using just one nanoscale material. However, highly durable and responsive sensors can be realized by combining zero-, one-, and two-dimensional nanomaterials on a flexible polymer substrate. For instance, in a screen-printable CNT/AgNP composite, the entangled CNTs connect the AgNPs to one another in a manner such that when a high strain is applied to the film, the measured distance between AgNPs is proportional to the measured resistance. This combination of 1D/0D nanomaterials is attractive because it enables a wide dynamic range in an AM-compatible paste that can realize a 7-fold improvement in sensitivity once printed (Fig. 7**a**) [184,188]. In an even more complex formulation, a ternary system of fullerenes, AgNWs, and GO addresses this challenge with each constituent species offering lubricity, high electrical conductivity, and brittle layered structure, respectively. This approach results in a working range of >50% strain and a gauge factor of >400% (Fig. 7**b**) [81].

These examples of engineered nanocomposite inks represent the first wave of highly sensitive nanomaterial-based sensors compatible with low-cost manufacturing techniques. Screen-printed sensors are ubiquitous in this literature space because contact-based AM techniques are low-cost, easily scalable to large dimensions, and conducive to higher nanomaterial loading [189–191]. Given these advantages, most multi-material nanocomposite sensors are currently screen-printed, and some of these screen-printed nanocomposite sensors are even more sensitive than their lithography-fabricated control devices [184,192]. The commercial availability of screen-printed electrodes has also enabled point-of-care technologies. With the integration of automatic screen printers, these nanocomposite inks can be adapted for one-step printing processes with a resolution of tens of microns.

Beyond screen printing, other deposition techniques to realize nanocomposite sensors from uncommon materials (e.g., magnetic NPs) are also being developed. For example, IJP and 3DP can be customized to achieve rapid magnetization of CNTs entangled with NiNPs in a printed pressure sensor, bypassing the lengthy incumbent process of covalent bonding [193]. CNTs have also been printed along with AgNPs via AJP in electrochemical protein sensors, exploiting the tolerance of AJP inks in a wide viscosity range (1–1000 cP), which better enables multi-material inks [194]. The use of AJP has also reduced device standard deviation from 50% to 10% when compared to screen printing [194].

3D-printable nanocomposites

Many compelling examples of nanocomposite sensors feature 0D metal and metal oxide NPs to realize stretchable conductors [195] and piezoelectric elements [79] for use in force sensors (Fig. 7**c**). Particularly for printed piezoelectrics, material innovations like thixotropic inks and conformal CNT coatings are enabling conductive devices with unprecedented form factors for controlled, multi-level 3D sensing [196]. Additionally, nanomaterial-loaded hydrogels can be engineered to be self-healing. Low-nanomaterial-loading (1–5 wt.%) composites exhibit the ability to recover from mechanical deformation by processes such as chemically induced alcoholysis of cross-linking bonds in certain polymers such as polyborosiloxane [197]. Other nanostructured polymer matrix materials include polyurethane and poly(lactic acid) (PU/PLA), which are primarily used in extrusion-based 3DP techniques such as fused deposition modeling; methacrylate co-polymers (PMMA) and polycaprolactone, commonly used in SLA methods; and epoxies, typically used in 3D IJP [40]. When paired with an active nanomaterial, binary nanocomposite inks with functional polymers as the matrix component offer nearly limitless materials platforms for manufacturing innovation.

For 1D/2D material polymer nanocomposites, extrusion printing of 3D sensing structures is a well-established technique, with 3D-printed CNT/polymer [195] and graphene/polymer [197] nanocomposites being reported in flexible sensing applications. However, process limitations on 3DP polymer-based nanocomposites include (1) discrepancies between the geometry of the computer-aided-design model and printed part due to material shrinkage or unwanted expansion, and (2) comparative absence of standardization and high-throughput analytical tools compared to conventional manufacturing processes [198]. Both challenges can be addressed by automated modeling, wherein machine learning algorithms facilitate iterative design that corrects for discrepancies in prototypical sensors transitioning to the manufacturing scale. Not only are 3DP techniques constructive, they are also informative, with structural analysis enabling high-throughput modeling and optimization for improved design fidelity in future prints [199]. Finally, some nanomaterial/polymer nanocomposite sensors are being realized via conventional IJP that hold promise for commercial IJP/3DP technology. If properly engineered for rapid ultraviolet (UV) curing, this would enable self-supporting form factors in 3D [79].

Like the way high-entropy, multi-component alloys have become a focal point in metallurgy, polynary nanocomposites have the potential to revolutionize the field of printed sensors. While each class of nanomaterials has its own limitations, clever combinations in heterostructures or nanocomposites can achieve synergistic performance (e.g., 1D NWs imparting electrical conductivity and 0D NPs imparting piezoelectricity or colloidal stability). With 3DP technology in a rapid acceleration stage, many futuristic applications are likely to be realized including tactile-responsive robotics, artificial organs with intrinsic disease-detection capabilities, and multifunctional prosthetics.

Future perspectives and research directions

Nanomaterials are intrinsically groundbreaking and conducive for AM, facilitating a plethora of ink formulations with (1) versatile physicochemical features and (2) synergistic effects from their composites that provide a materials-driven toolbox for various sensing systems upon printing. Each sub-class of nanomaterials lends unique structure- and composition-driven properties to the sensing modalities: highly conductive 0D AgNPs are

Please cite this article in press as: X. Sui et al., Materials Today, (2021), https://doi.org/10.1016/j.mattod.2021.02.001

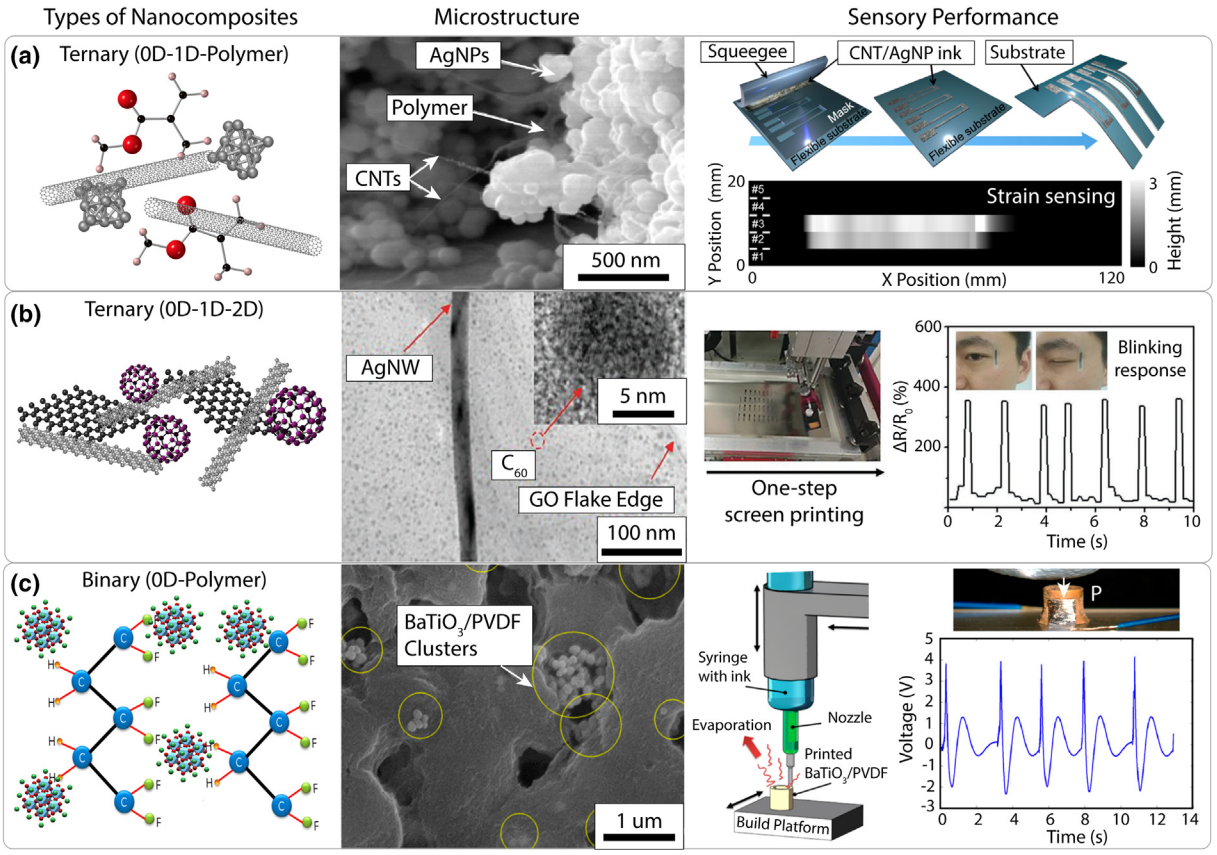

FIG. 7

Multi-material printed nanocomposites for next-generation, deformable tactile sensors. (a) Fully printed, highly sensitive, multifunctional artificial electronic whisker arrays integrated with strain and temperature sensors. Reproduced with permission from [184]. Copyright © 2014 American Chemical Society. (b) 0D-1D-2D ternary nanocomposite-based strain sensor designed to lower internal friction and boost sensing performance. Reproduced with permission from [81]. Copyright © 2018 WILEY-VCH Verlag GmbH & Co. KGaA, Weinheim. (c) One-step, solvent-evaporation-assisted 3D printing of piezoelectric PVDF nanocomposite structures. Reproduced with permission from [79]. Copyright © 2017 American Chemical Society.

widely used in printing circuits of sensor devices [96,200]; robust, printed 1D CNT networks are employed in wearable sensors [82]; photosensitive 2D MoS_2 and BP nanosheets are processed into photodetectors [13,14]; and soft materials form composite sensors for flexible electronics [26,169]. Meanwhile, AM enables on-demand patterning and integration of all classes of nanomaterials into functional sensors at a low cost. Contact, non-contact, and mixed-contact material printing approaches have distinct capabilities and advantages, requiring tailored rheological properties of the inks to maintain stable printing at a high resolution. Contact printing methods (e.g., screen and gravure printing) demand more viscous inks and offer high-throughput, low-cost production, while non-contact approaches (e.g., IJP, AJP, and 3DP) are characterized by economical, drop-on-demand material deposition. Both systematic selection of nanomaterials and a suitable printing approach should be carefully considered when mapping the next decade of sensor research (Fig. 8).

In addition to on-demand patterning of materials, the efficient integration capabilities of AM are highly attractive for fabricating multi-component devices. In commercial sensing devices, several complementary materials with distinct functions operate synergistically. For example, digitally printing techniques like IJP can fabricate complex MoS_2 and graphene patterns in sequence and overlap them to realize an integrated photodetector [165]. A three-layered infrared photodetector using stabilized PbS nanocrystals as the photoreceptor (Fig. 8**a**) [93] and multiplexed biosensors with a conductive hydrogel matrix [172] have also been integrated by several iterations of IJP. Moreover, smart packaging achieved by integrating humidity sensing with interactive signage is enabled by a R2R gravure printing scheme consisting of 5 printing layers and 4 coating layers [104]. This pioneering work reveals the powerful manufacturing and integration capabilities of AM for fully printed sensing systems in the future.

In the past decade, significant progress has been achieved for AM of nanomaterials in different types of sensors (e.g., force, temperature, light, chemical, and pH sensors). Future efforts should focus on developing multifunctional devices to meet the urgent demands of e-skins, human–machine interfaces, and point-of-care diagnostics and therapies. For example, this Review has highlighted the highly sensitive response of CNT-AgNP and CNT-PEDOT:PSS composites to tactile stimuli and temperature changes, respectively, in screen-printed sensors [184,188]. However, it will be more challenging to integrate multiple sensing components onto a single platform to realize

Please cite this article in press as: X. Sui et al., Materials Today, (2021), https://doi.org/10.1016/j.mattod.2021.02.001

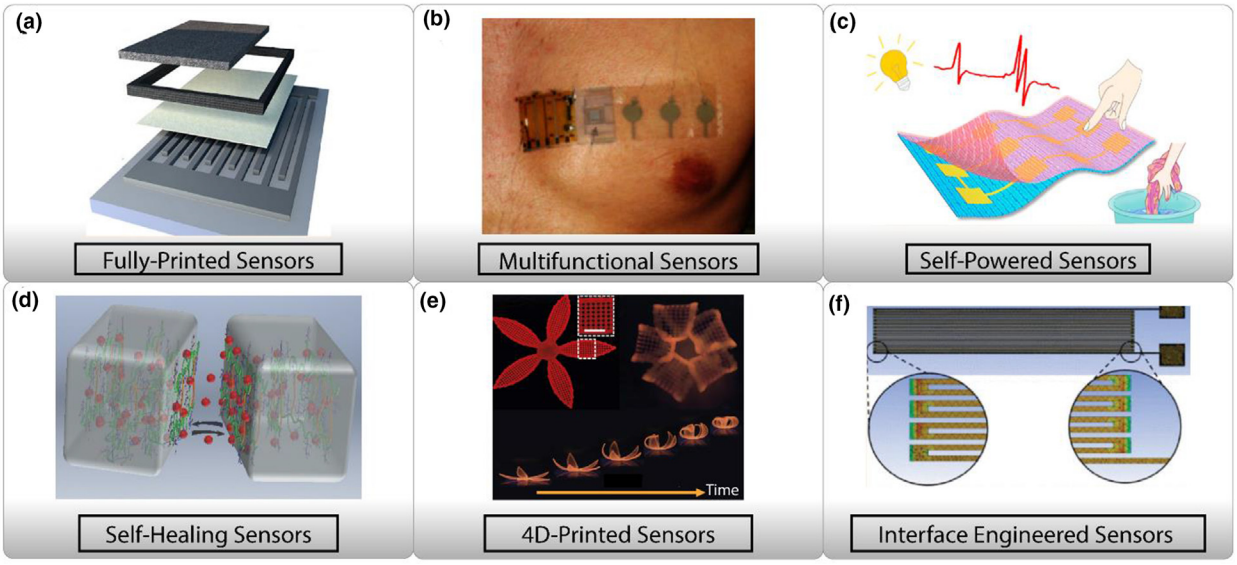

FIG. 8

Emerging applications and future research thrusts for printed nanomaterial-based sensors. (a) Fully printed sensors with high photosensitivity. Reproduced with permission from [93]. Copyright © 2019 American Chemical Society. (b) Multifunctional health care monitoring systems. Reproduced with permission from [78]. Copyright © 2016 The Authors, AAAS under a CC BY-NC license. (c) Self-powered touch/gesture tribo-sensors. Reproduced with permission from [82]. Copyright © 2017 American Chemical Society. (d) Self-healing hydrogels with high pressure sensitivity. Reproduced with permission from [174]. Copyright © 2017 WILEY-VCH Verlag GmbH & Co. KGaA, Weinheim. (e) Biomimetic 4D printing. Reproduced with permission from [25]. Copyright © 2016 Springer Nature. (f) Interface engineering for improved sensor performance. Reproduced with permission from [87]. Copyright © 2018 IEEE.

system-level multifunctionalities such as point-of-care health monitoring and e-skin [78]. A feasible and economic route is modular device design with several detachable components before AM of the entire device system is realized. Aligned with this vision, a health care monitoring system has been designed with two detachable components: one component is disposable, which integrates printed temperature, acceleration and electrocardiogram sensors onto a flexible substrate, and another component is reusable containing more expensive material (Fig. 8**b**) [78]. In this configuration electronically advanced, silicon-based integrated circuits can be combined with reusable device components for sophisticated signal processing [78], while liquid metals such as eutectic gallium indium (eGaIn) can be used to provide flexible, stable and reversible contacts between detachable components [201].

Furthermore, while printed sensing devices can be easily powered by external power sources for demonstration in laboratories, integrated power is indispensable for scalable integration. A promising approach is to combine power sources such as supercapacitors [141], biofuels [189], and nanogenerators [202] with sensing components into a single device, enabling simple structures, easy fabrication, and excellent stability [82]. Towards this end, triboelectric nanogenerators (Fig. 8**c**) [82], printed piezoelectric nanostructures [70] and printed biofuel cells [189] are all viable strategies for paradigm-shifting, off-grid sensing modalities. The realization and integration of other printed energy conversion and storage devices (e.g., photovoltaics and batteries) provide another pathway to integrated power.

For specific applications of flexible sensing systems in wearable electronics, self-healing capabilities are highly desirable to improve device durability during bending and stretching (Fig. 8**d**) [174]. Printable self-healing hydrogels are the most promising material platforms to date due to their flexibility, chemical functionality, and broad nanomaterial compatibility. Such self-healing behavior can be realized through dynamic hydrogen bonds [187], ionic interactions [174], and boron/oxygen bonds [197]. Furthermore, electrical conductivity can be enhanced by using intrinsically conductive polymers (e.g., PPy [174]) or by adding other conductive nanomaterials (e.g., CNTs [203] and graphene [197]) to the matrix. Ion transport can also be incorporated through nanocomposite ionogel-based materials [204], including those that employ 2D nanomaterials such as hexagonal boron nitride [205]. These tunable electrical and ionic properties will greatly expand the applications of self-healing materials, from conductive circuits to stimuli-responsive (e.g., mechanical [174] and chemical [197]) components in printed sensors.

AM can also be used to program specific configurations or functionalities in 3DP sensors over time in response to environmental stimuli via so-called four-dimensional (4D) printing (Fig. 8**e**) [25,206,207]. In these nascent systems, anisotropic strain environments drive adaptations of the printed structures, but only with limited response mechanisms confined to polymer-based composites [208]. By expanding the capabilities of 4D-printing, sensing platforms driven by minimalistic device structures in the absence of conductive electrodes and power systems may become tenable. Further fundamental studies towards the nature of the interfaces between substrates and printed nanomaterial structures, as well as the interfaces between different printed electrical components, are also critical to improve sensing performance. Interfacial energy between substrates and printed structures plays an important role in pattern formation

Please cite this article in press as: X. Sui et al., Materials Today, (2021), https://doi.org/10.1016/j.mattod.2021.02.001

[209], and subsequently impacts device figures of merit (e.g., sensitivity, stability) [87]. Furthermore, interfaces between printed electrical components originating from different functional inks lead to increased contact resistance, limiting the electrical performance of FET-based sensors and patterned contacts [128]. Thus, interface engineering will significantly improve sensor performance in terms of electrical properties, stability, and sensitivity (Fig. 8**f**).

With the deployment of smart objects within IoT, sensing platforms will penetrate almost all aspects of our daily lives. AM of nanomaterial functional inks offers a versatile, efficient, and low-cost approach for industrial-scale sensor fabrication and integration. Meanwhile, AM is being revolutionized by automated techniques that will boost production efficiency, drive down integration costs, and minimize device variation. Indeed, mass production of low-cost sensors with high uniformity will enable simultaneous detection by arrays of nanomaterial-based sensors in parallel, offering statistical reliability and accuracy. These attributes are particularly important amid massive public health crises such as the ongoing SARS-CoV-2/COVID-19 pandemic, which demands rapid, low-cost, and point-of-care virus detection that can be administered outside of laboratories. Emerging sensor technologies enabled by the unique attributes of AM present a paradigm shift for materials scientists, chemists, and electrical engineers to develop previously untenable nanomaterial-based sensing platforms at the industrial scale.

Declaration of Competing Interest

The authors declare that they have no known competing financial interests or personal relationships that could have appeared to influence the work reported in this paper.

Acknowledgments

This work was supported by the National Science Foundation Scalable Nanomanufacturing Program (NSF CMMI-1727846 and NSF CMMI-2039268) and the Future Manufacturing Program (NSF CMMI-2037026).

References

[1] F.G. Bănică, Chemical Sensors and Biosensors: Fundamentals and Applications, John Wiley & Sons, 2012.
[2] V.K. Khanna, Nanosensors: Physical, Chemical, and Biological, CRC Press, Boca Raton, FL, 2012.
[3] E. Singh, H.S. Nalwa (Eds.), Nanomaterial-based Flexible and Multifunctional Sensors, American Scientific Publishers, Los Angeles, CA, 2019.
[4] K. Kostarelos, K.S. Novoselov, Nat. Nanotechnol. 9 (2014) 744–745, https://doi.org/10.1038/nnano.2014.224.
[5] D. Bonifazi, O. Enger, F. Diederich, Chem. Soc. Rev. 36 (2007) 390–414, https://doi.org/10.1039/B604308A.
[6] J. Herrmann et al., Appl. Phys. Lett. 91 (2007) 183105, https://doi.org/10.1063/1.2805026.
[7] Z. Yue et al., ACS Appl. Mater. Interfaces 5 (2013) 2800–2814, https://doi.org/10.1021/am3028662.
[8] D.J. Lipomi et al., Nat. Nanotechnol. 6 (2011) 788–792, https://doi.org/10.1038/nnano.2011.184.
[9] R.P. Tortorich, E. Song, J.-W. Choi, J. Electrochem. Soc. 161 (2014) B3044–B3048, https://doi.org/10.1149/2.008402jes.
[10] J. Chen et al., Sens. Actuators B: Chem. 281 (2019) 1080–1087, https://doi.org/10.1016/j.snb.2018.10.035.
[11] Y. Cui, Science 293 (2001) 1289–1292, https://doi.org/10.1126/science.1062711.
[12] V. Dua et al., Angew. Chem. Int. 49 (2010) 2154–2157, https://doi.org/10.1002/anie.v49:1210.1002/anie.200905089.
[13] J. Li et al., Adv. Funct. Mater. 24 (2014) 6524–6531, https://doi.org/10.1002/adfm.v24.4110.1002/adfm.201400984.
[14] G. Hu et al., Nat. Commun. 8 (2017), https://doi.org/10.1038/s41467-017-00358-1.
[15] A. Sinha et al., Anal. Chem. 105 (2018) 424–435, https://doi.org/10.1016/j.trac.2018.05.021.
[16] C. Wang et al., Adv. Mater. 30 (2018) 1801368, https://doi.org/10.1002/adma.201801368.
[17] E. Danesh et al., Anal. Chem. 86 (2014) 8951–8958, https://doi.org/10.1021/ac501908c.
[18] M. Mayer, A.J. Baeumner, Chem. Rev. 119 (2019) 7996–8027, https://doi.org/10.1021/acs.chemrev.8b00719.
[19] K. Chen et al., Adv. Mater. 28 (2016) 4397–4414, https://doi.org/10.1002/adma.201504958.
[20] Y.S. Rim et al., Adv. Mater. 28 (2016) 4415–4440, https://doi.org/10.1002/adma.201505118.
[21] M. Kuang et al., Adv. Opt. Mater. 2 (2014) 34–38, https://doi.org/10.1002/adom.201300369.
[22] X. Cao et al., ACS Nano 10 (2016) 9816–9822, https://doi.org/10.1021/acsnano.6b05368.
[23] Z. Chu, J. Peng, W. Jin, Sens. Actuators B: Chem. 243 (2017) 919–926, https://doi.org/10.1016/j.snb.2016.12.022.
[24] B. Kannan et al., Anal. Chem. 87 (2015) 9288–9293, https://doi.org/10.1021/acs.analchem.5b01923.
[25] A. Sydney Gladman et al., Nat. Mater. 15 (2016) 413–418, https://doi.org/10.1038/nmat4544.
[26] S. Jung et al., Adv. Mater. 26 (2014) 4825–4830, https://doi.org/10.1002/adma.201401364.
[27] W. Yang et al., Adv. Mater. Technol. 3 (2018) 1700241, https://doi.org/10.1002/admt.201700241.
[28] J.T. Muth et al., Adv. Mater. 26 (2014) 6307–6312, https://doi.org/10.1002/adma.201400334.
[29] S. Khan, L. Lorenzelli, R.S. Dahiya, IEEE Sens. J. 15 (2015) 3164–3185, https://doi.org/10.1109/JSEN.2014.2375203.
[30] W.J. Hyun et al., Adv. Mater. 27 (2015) 109–115, https://doi.org/10.1002/adma.201404133.
[31] M.A. Meitl et al., Nat. Mater. 5 (2006) 33–38, https://doi.org/10.1038/nmat1532.
[32] P. Andrich et al., Nano Lett. 18 (2018) 4684–4690, https://doi.org/10.1021/acs.nanolett.8b00895.
[33] M. Bariya et al., ACS Nano 12 (2018) 6978–6987, https://doi.org/10.1021/acsnano.8b02505.
[34] A.K. Assaifan et al., ACS Appl. Mater. Interfaces 8 (2016) 33802–33810, https://doi.org/10.1021/acsami.6b11640.
[35] B. Derby, Annu. Rev. Mater. Res. 40 (2010) 395–414, https://doi.org/10.1146/annurev-matsci-070909-104502.
[36] T.Q. Trung, N.-E. Lee, Adv. Mater. 28 (2016) 4338–4372, https://doi.org/10.1002/adma.201504244.
[37] J.-U. Park et al., Nano Lett. 10 (2010) 584–591, https://doi.org/10.1021/nl903495f.
[38] A. Mahajan, C.D. Frisbie, L.F. Francis, ACS Appl. Mater. Interfaces 5 (2013) 4856–4864, https://doi.org/10.1021/am400606y.
[39] F.S. Gittleson et al., ACS Nano 9 (2015) 10005–10017, https://doi.org/10.1021/acsnano.5b03578.
[40] M. Nadgorny, A. Ameli, ACS Appl. Mater. Interfaces 10 (2018) 17489–17507, https://doi.org/10.1021/acsami.8b01786.
[41] C.M. Homenick et al., ACS Appl. Mater. Interfaces 8 (2016) 27900–27910, https://doi.org/10.1021/acsami.6b06838.
[42] G. Hu et al., Chem. Soc. Rev. 47 (2018) 3265–3300, https://doi.org/10.1039/C8CS00084K.
[43] S. Zhang et al., Chem. Rev. 117 (2017) 12942–13038, https://doi.org/10.1021/acs.chemrev.7b00088.
[44] T.Q. Trung, N.-E. Lee, Adv. Mater. 29 (2017) 1603167, https://doi.org/10.1002/adma.201603167.
[45] Y. Yang, W. Gao, Chem. Soc. Rev. 48 (2019) 1465–1491, https://doi.org/10.1039/C7CS00730B.
[46] Y. Liu et al., Chem. Rev. 117 (2017) 12893–12941, https://doi.org/10.1021/acs.chemrev.7b00291.
[47] Z. Bao, X. Chen, Adv. Mater. 28 (2016) 4177–4179, https://doi.org/10.1002/adma.201601422.
[48] C.C. Yeh, H.W. Zan, O. Soppera, Adv. Mater. 30 (2018) 1800923, https://doi.org/10.1002/adma.201800923.

Please cite this article in press as: X. Sui et al., Materials Today, (2021), https://doi.org/10.1016/j.mattod.2021.02.001

[49] X. Yu et al., Adv. Mater. 30 (2018) 1707624, https://doi.org/10.1002/adma.201707624.
[50] J.H. Koo et al., Adv. Funct. Mater. 28 (2018) 1801834, https://doi.org/10.1002/adfm.201801834.
[51] K. Fukuda, T. Someya, Adv. Mater. 29 (2017) 1602736, https://doi.org/10.1002/adma.201602736.
[52] Y. Huang et al., Adv. Funct. Mater. 29 (2019) 1808509, https://doi.org/10.1002/adfm.201808509.
[53] W. Wu, Nanoscale 9 (2017) 7342–7372, https://doi.org/10.1039/C7NR01604B.
[54] S. Zhao et al., Adv. Funct. Mater. 9 (2017) 12147–12164, https://doi.org/10.1021/acsami.6b13800.
[55] S.-T. Han et al., Adv. Mater. 29 (2017) 1700375, https://doi.org/10.1002/adma.201700375.
[56] R. Singh, E. Singh, H.S. Nalwa, RSC Adv. 7 (2017) 48597–48630, https://doi.org/10.1039/C7RA07191D.
[57] T.-T. Huang, W. Wu, Adv. Mater. Interfaces 7 (2020) 2000015, https://doi.org/10.1002/admi.202000015.
[58] Y. Sui, C.A. Zorman, J. Electrochem. Soc. 167 (2020) 037571, https://doi.org/10.1149/1945-7111/ab721f.
[59] S. Khan, S. Ali, A. Bermak, Sensors 19 (2019) 1230, https://doi.org/10.3390/s19051230.
[60] S.F. Kamarudin, M. Mustapha, J.-K. Kim, Polym. Rev. 61 (2021) 116–156, https://doi.org/10.1080/15583724.2020.1729180.
[61] S. Choi et al., Adv. Mater. 28 (2016) 4203–4218, https://doi.org/10.1002/adma.201504150.
[62] Y. Liu, M. Pharr, G.A. Salvatore, ACS Nano 11 (2017) 9614–9635, https://doi.org/10.1021/acsnano.7b04898.
[63] T.R. Ray et al., Chem. Rev. 119 (2019) 5461–5533, https://doi.org/10.1021/acs.chemrev.8b00573.
[64] M. Amjadi et al., Adv. Funct. Mater. 26 (2016) 1678–1698, https://doi.org/10.1002/adfm.201504755.
[65] T. Cheng et al., Adv. Mater. 27 (2015) 3349–3376, https://doi.org/10.1002/adma.201405864.
[66] E. Jabari et al., 2D Mater. 6 (2019) 042004, https://doi.org/10.1088/2053-1583/ab29b2.
[67] C. Gong et al., Adv. Funct. Mater. 28 (2018) 1706559, https://doi.org/10.1002/adfm.201706559.
[68] F. Bonaccorso et al., Adv. Mater. 28 (2016) 6136–6166, https://doi.org/10.1002/adma.201506410.
[69] Z. Ma et al., Nano Lett. 18 (2018) 4570–4575, https://doi.org/10.1021/acs.nanolett.8b01825.
[70] Y. Huang et al., Nano Energy 40 (2017) 432–439, https://doi.org/10.1016/j.nanoen.2017.07.048.
[71] B. Creran et al., ACS Appl. Mater. Interfaces 6 (2014) 19525–19530, https://doi.org/10.1021/am505689g.
[72] L. Huang et al., ACS Appl. Mater. Interfaces 6 (2014) 7426–7433, https://doi.org/10.1021/am500843p.
[73] A. Yakoh et al., ACS Appl. Mater. Interfaces 10 (2018) 20775–20782, https://doi.org/10.1021/acsami.8b04883.
[74] A. Chałupniak, A. Merkoçi, ACS Appl. Mater. Interfaces 9 (2017) 44766–44775, https://doi.org/10.1021/acsami.7b12368.
[75] J. Hou et al., Angew. Chem. Int. 53 (2014) 5791–5795, https://doi.org/10.1002/anie.201400686.
[76] N. Chauhan et al., ACS Appl. Mater. Interfaces 10 (2018) 30631–30639, https://doi.org/10.1021/acsami.8b08901.
[77] J.S. Dudani et al., Adv. Funct. Mater. 26 (2016) 2919–2928, https://doi.org/10.1002/adfm.201505142.
[78] Y. Yamamoto et al., Sci. Adv. 2 (2016) e1601473, https://doi.org/10.1126/sciadv.1601473.
[79] S. Bodkhe et al., ACS Appl. Mater. Interfaces 9 (2017) 20833–20842, https://doi.org/10.1021/acsami.7b04095.
[80] J.H. Song et al., Adv. Mater. 29 (2017) 1702625, https://doi.org/10.1002/adma.201702625.
[81] X. Shi et al., Adv. Funct. Mater. 28 (2018) 1800850, https://doi.org/10.1002/adfm.201800850.
[82] R. Cao et al., ACS Nano 12 (2018) 5190–5196, https://doi.org/10.1021/acsnano.8b02477.
[83] E. Roh et al., Adv. Mater. 29 (2017) 1703004, https://doi.org/10.1002/adma.201703004.
[84] M. Segev-Bar, H. Haick, ACS Nano 7 (2013) 8366–8378, https://doi.org/10.1021/nn402728g.
[85] X. Luo et al., Electroanalysis 18 (2006) 319–326, https://doi.org/10.1002/elan.200503415.
[86] Z. Farka et al., Chem. Rev. 117 (2017) 9973–10042, https://doi.org/10.1021/acs.chemrev.7b00037.
[87] S. Agarwala, G.L. Goh, W.Y. Yeong, IEEE Access 6 (2018) 63080–63086, https://doi.org/10.1109/ACCESS.2018.2876647.
[88] J. Kim et al., Biosens. Bioelectron. 74 (2015) 1061–1068, https://doi.org/10.1016/j.bios.2015.07.039.
[89] S. Ali et al., Langmuir 32 (2016) 11432–11439, https://doi.org/10.1021/acs.langmuir.6b02885.
[90] L. Cheng et al., ACS Appl. Mater. Interfaces 10 (2018) 34869–34877, https://doi.org/10.1021/acsami.8b10252.
[91] G. Dubourg, M. Radović, ACS Appl. Mater. Interfaces 11 (2019) 6257–6266, https://doi.org/10.1021/acsami.8b19976.
[92] M. Santhiago et al., ACS Appl. Mater. Interfaces. 9 (2017) 24365–24372, https://doi.org/10.1021/acsami.7b06598.
[93] A. YousefiAmin et al., ACS Nano 13 (2019) 2389–2397, https://doi.org/10.1021/acsnano.8b09223.
[94] K. Kim et al., Nano Energy 41 (2017) 301–307, https://doi.org/10.1016/j.nanoen.2017.09.024.
[95] X. Liu et al., Nat. Commun. 5 (2014) 4007, https://doi.org/10.1038/ncomms5007.
[96] R. Guo et al., Adv. Sci. 2 (2015) 1400021, https://doi.org/10.1002/advs.201400021.
[97] E. Homede et al., Adv. Funct. Mater. 26 (2016) 6359–6370, https://doi.org/10.1002/adfm.201602326.
[98] B. Ketelsen et al., ACS Appl. Mater. Interfaces 10 (2018) 37374–37385, https://doi.org/10.1021/acsami.8b12057.
[99] Y. Qin et al., Adv. Funct. Mater. 26 (2016) 4923–4933, https://doi.org/10.1002/adfm.201600657.
[100] W. Shou et al., Adv. Mater. 29 (2017) 1700172, https://doi.org/10.1002/adma.201700172.
[101] W. Zhao et al., ACS Nano 9 (2015) 6168–6177, https://doi.org/10.1021/acsnano.5b02704.
[102] Y. Lin et al., Adv. Mater. 31 (2019) 1804285, https://doi.org/10.1002/adma.201804285.
[103] C. Yeom et al., Adv. Mater. 27 (2015) 1561–1566, https://doi.org/10.1002/adma.201404850.
[104] H. Kang et al., Sci. Rep. 4 (2015) 5387, https://doi.org/10.1038/srep05387.
[105] Y.S. Rim et al., ACS Nano 9 (2015) 12174–12181, https://doi.org/10.1021/acsnano.5b05325.
[106] Z. Chen et al., Nano Energy 27 (2016) 78–86, https://doi.org/10.1016/j.nanoen.2016.06.048.
[107] A.F. Sartori et al., Small 15 (2019) 1803774, https://doi.org/10.1002/smll.201803774.
[108] L. Bai et al., ACS Nano 8 (2014) 11094–11100, https://doi.org/10.1021/nn504659p.
[109] I. Naydenova et al., Chem. Mater. 27 (2015) 6097–6101, https://doi.org/10.1021/acs.chemmater.5b02629.
[110] T.-H. Kim et al., ACS Nano 11 (2017) 5992–6003, https://doi.org/10.1021/acsnano.7b01894.
[111] P. Yang, R. Yan, M. Fardy, Nano Lett. 10 (2010) 1529–1536, https://doi.org/10.1021/nl100665r.
[112] Z. Yang, X. Dou, Adv. Funct. Mater. 26 (2016) 2406–2425, https://doi.org/10.1002/adfm.201504846.
[113] G. Lu, L.E. Ocola, J. Chen, Adv. Mater. 21 (2009) 2487–2491, https://doi.org/10.1002/adma.200803536.
[114] J. Li et al., Adv. Funct. Mater. 17 (2007) 3207–3215, https://doi.org/10.1002/adfm.200700065.
[115] M.R. Ayatollahi et al., Polym. Test. 30 (2011) 548–556, https://doi.org/10.1016/j.polymertesting.2011.04.008.
[116] K. Kim et al., Adv. Mater. 31 (2019) 1804690, https://doi.org/10.1002/adma.201804690.
[117] B.Q. Wei, R. Vajtai, P.M. Ajayan, Appl. Phys. Lett. 79 (2001) 1172–1174, https://doi.org/10.1063/1.1396632.
[118] W. Yang et al., Energy Environ. Sci. 12 (2019) 1605–1612, https://doi.org/10.1039/C9EE00536F.
[119] W.A. Gaviria Rojas, M.C. Hersam, Adv. Mater. 32 (2020) 1905654, https://doi.org/10.1002/adma.201905654.
[120] B. Peng et al., Nat. Nanotechnol. 3 (2008) 626–631, https://doi.org/10.1038/nnano.2008.211.
[121] A.J. Bandodkar et al., Nano Lett. 16 (2016) 721–727, https://doi.org/10.1021/acs.nanolett.5b04549.
[122] J.H. Kim et al., ACS Nano 10 (2016) 8879–8887, https://doi.org/10.1021/acsnano.6b04771.

Please cite this article in press as: X. Sui et al., Materials Today, (2021), https://doi.org/10.1016/j.mattod.2021.02.001

[123] J. Dong et al., ACS Nano 12 (2018) 3769–3779, https://doi.org/10.1021/acsnano.8b00980.
[124] L. Wang et al., Adv. Mater. 31 (2019) 1804583, https://doi.org/10.1002/adma.201804583.
[125] W. Deng et al., Adv. Mater. 28 (2016) 2201–2208, https://doi.org/10.1002/adma.201505126.
[126] S. Yao, et al., Adv. Healthc. Mater. 6 (2017) https://doi.org/10.1002/adhm.201601159.
[127] Q. Zhang et al., Small 9 (2013) 1237–1265, https://doi.org/10.1002/smll.201203252.
[128] C. Cao, J.B. Andrews, A.D. Franklin, Adv. Electron. Mater. 3 (2017) 1700057, https://doi.org/10.1002/aelm.201700057.
[129] X. Wang et al., ACS Appl. Mater Interfaces 10 (2018) 7371–7380, https://doi.org/10.1021/acsami.7b17766.
[130] T.-H. Kang et al., Nano Lett. 19 (2019) 3684–3691, https://doi.org/10.1021/acs.nanolett.9b00764.
[131] T.-S. Kim et al., Nano Energy 58 (2019) 437–446, https://doi.org/10.1016/j.nanoen.2019.01.052.
[132] A.S.R. Bati et al., Nanoscale 10 (2018) 22087–22139, https://doi.org/10.1039/C8NR07379A.
[133] J.W. Jeong et al., Nat. Commun. 5 (2014) 5387, https://doi.org/10.1038/ncomms6387.
[134] M.A. Green, A. Ho-Baillie, H.J. Snaith, Nat. Photon. 8 (2014) 506–514, https://doi.org/10.1038/nphoton.2014.134.
[135] C.R. Ryder et al., ACS Nano 10 (2016) 3900–3917, https://doi.org/10.1021/acsnano.6b01091.
[136] H. Lee et al., Nature Nanotechnol. 11 (2016) 566–572, https://doi.org/10.1038/nnano.2016.38.
[137] J. Liu et al., Adv. Funct. Mater. 29 (2019) 1807326, https://doi.org/10.1002/adfm.201807326.
[138] D. McManus et al., Nat. Nanotechnol. 12 (2017) 343–350, https://doi.org/10.1038/nnano.2016.281.
[139] Q. He et al., Chem. Sci. 3 (2012) 1764, https://doi.org/10.1039/c2sc20205k.
[140] T. Vuorinen et al., Sci. Rep. 6 (2016) 35289, https://doi.org/10.1038/srep35289.
[141] L. Yu et al., Nano Res. 12 (2019) 331–338, https://doi.org/10.1007/s12274-018-2219-1.
[142] J.A. Hondred et al., ACS Appl. Mater. Interfaces 10 (2018) 11125–11134, https://doi.org/10.1021/acsami.7b19763.
[143] K. Parate et al., ACS Appl. Mater. Interfaces 12 (2020) 8592–8603, https://doi.org/10.1021/acsami.9b22183.
[144] D. Ji et al., Biosens. Bioelectron. 129 (2019) 216–223, https://doi.org/10.1016/j.bios.2018.09.082.
[145] M.K. Choi et al., Adv. Funct. Mater. 25 (2015) 7109–7118, https://doi.org/10.1002/adfm.201502956.
[146] Y. Su et al., Nano Research 8 (2015) 3954–3962, https://doi.org/10.1007/s12274-015-0897-5.
[147] Z. Wang et al., Adv. Funct. Mater. 28 (2018) 1707043, https://doi.org/10.1002/adfm.201707043.
[148] M.G. Chung et al., Sens. Actuators B. Chem. 166–167 (2012) 172–176, https://doi.org/10.1016/j.snb.2012.02.036.
[149] C.Y. Hui et al., Angew. Chem. Int. 57 (2018) 4549–4553, https://doi.org/10.1002/anie.201712903.
[150] L. Baptista-Pires et al., ACS Nano 10 (2016) 853–860, https://doi.org/10.1021/acsnano.5b05963.
[151] S. Xu et al., Nano Energy 50 (2018) 479–488, https://doi.org/10.1016/j.nanoen.2018.05.064.
[152] S. Manzeli et al., Nat. Rev. Mater. 2 (2017) 17033, https://doi.org/10.1038/natrevmats.2017.33.
[153] Y. Wei et al., ACS Appl. Mater. Interfaces 11 (2019) 21445–21453, https://doi.org/10.1021/acsami.9b01515.
[154] D.J. Late, T. Doneux, M. Bougouma, Appl. Phys. Lett. 105 (2014) 233103, https://doi.org/10.1063/1.4903358.
[155] K.Y. Ko et al., ACS Appl. Mater. Interfaces 10 (2018) 23910–23917, https://doi.org/10.1021/acsami.8b07034.
[156] J. Kang et al., ACS Nano 9 (2015) 3596–3604, https://doi.org/10.1021/acsnano.5b01143.
[157] J. Kang et al., Proc. Natl. Acad. Sci. USA 113 (2016) 11688–11693, https://doi.org/10.1073/pnas.1602215113.
[158] J.D. Wood et al., Nano. Lett. 14 (2014) 6964–6970, https://doi.org/10.1021/nl5032293.
[159] C.R. Ryder et al., Nat. Chem. 8 (2016) 597–602, https://doi.org/10.1038/nchem.2505.
[160] S. Cui, Nat. Commun. 6 (2015), https://doi.org/10.1038/ncomms9632.
[161] T.H. Osborn, A.A. Farajian, Nano Res. 7 (2014) 945–952, https://doi.org/10.1007/s12274-014-0454-7.
[162] W. Hu, Phys. Chem. Chem. Phys. 16 (2014) 6957, https://doi.org/10.1039/c3cp55250k.
[163] V. Shukla et al., J. Phys. Chem. C 121 (2017) 26869–26876, https://doi.org/10.1021/acs.jpcc.7b09552.
[164] A. Shahbazi Kootenaei, G. Ansari, Phys. Lett. A 380 (2016) 2664–2668, https://doi.org/10.1016/j.physleta.2016.06.016.
[165] J.-W.T. Seo et al., ACS Appl. Mater. Interfaces 11 (2019) 5675–5681, https://doi.org/10.1021/acsami.8b19817.
[166] H. Shirakawa et al., J. Chem. Soc., Chem. Commun. (1977) 578–580, https://doi.org/10.1039/c39770000578.
[167] N. Kim, et al., Adv. Mater. 26 (2014) 2268-2272, 2109. https://doi.org/10.1002/adma.201304611.
[168] F. Zhang et al., Nat. Commun. 6 (2015) 8356, https://doi.org/10.1038/ncomms9356.
[169] L.V. Kayser, D.J. Lipomi, Adv. Mater. 31 (2019), https://doi.org/10.1002/adma.201806133.
[170] Y. Chen et al., Sci. Adv. 3 (2017) e1701629, https://doi.org/10.1126/sciadv.1701629.
[171] J.U. Lind et al., Nat. Mater. 16 (2017) 303–308, https://doi.org/10.1038/nmat4782.
[172] L. Li et al., Nano Lett. 18 (2018) 3322–3327, https://doi.org/10.1021/acs.nanolett.8b00003.
[173] X.-Y. Yin et al., Mater. Horiz. 6 (2019) 767–780, https://doi.org/10.1039/C8MH01398E.
[174] M.A. Darabi et al., Adv. Mater. 29 (2017) 1700533, https://doi.org/10.1002/adma.201700533.
[175] S.G. Bucella et al., Nat. Commun. 6 (2015), https://doi.org/10.1038/ncomms9394.
[176] G. Kamita et al., Adv. Opt. Mater. 4 (2016) 1950–1954, https://doi.org/10.1002/adom.201600451.
[177] H.-L. Liang et al., Nat. Commun. 9 (2018) 4632, https://doi.org/10.1038/s41467-018-07048-6.
[178] R. Jia et al., Nat. Commun. 10 (2019) 1–10, https://doi.org/10.1038/s41467-019-08675-3.
[179] C. Chang et al., Nano Lett. 10 (2010) 726–731, https://doi.org/10.1021/nl9040719.
[180] D. Jariwala, T.J. Marks, M.C. Hersam, Nat. Mater. 16 (2017) 170–181, https://doi.org/10.1038/nmat4703.
[181] S. Padgaonkar et al., Acc. Chem. Res. 53 (2020) 763–772, https://doi.org/10.1021/acs.accounts.9b00581.
[182] S. Lim et al., Adv. Funct. Mater. 25 (2015) 375–383, https://doi.org/10.1002/adfm.201402987.
[183] S.-W. Hwang et al., Nano Lett. 15 (2015) 2801–2808, https://doi.org/10.1021/nl503997m.
[184] S. Harada et al., ACS Nano 8 (2014) 12851–12857, https://doi.org/10.1021/nn506293y.
[185] S.J. Kim et al., ACS Nano 9 (2015) 2677–2688, https://doi.org/10.1021/nn5064634.
[186] M. Gong et al., ACS Appl. Mater. Interfaces 9 (2017) 27801–27808, https://doi.org/10.1021/acsami.7b08226.
[187] W. Huang et al., Adv. Funct. Mater. 25 (2015) 3745–3755, https://doi.org/10.1002/adfm.201404228.
[188] S. Harada et al., ACS Nano 8 (2014) 3921–3927, https://doi.org/10.1021/nn500845a.
[189] I. Jeerapan et al., J. Mater. Chem. A 4 (2016) 18342–18353, https://doi.org/10.1039/C6TA08358G.
[190] R. Ma, V.V. Tsukruk, Adv. Funct. Mater. 27 (2017) 1604802, https://doi.org/10.1002/adfm.201604802.
[191] A. Abellán-Llobregat et al., Biosens. Bioelectron. 91 (2017) 885–891, https://doi.org/10.1016/j.bios.2017.01.058.
[192] W. Honda et al., Adv. Funct. Mater. 24 (2014) 3298, https://doi.org/10.1002/adfm.201470144.
[193] A.R. Abdel Fattah et al., ACS Appl. Mater. Interfaces 8 (2016) 1589–1593, https://doi.org/10.1021/acsami.5b11700.
[194] E. Cantù et al., Sensors 18 (2018) 1–14, https://doi.org/10.3390/s18113719.
[195] S.-Z. Guo et al., Adv. Mater. 29 (2017) 1701218, https://doi.org/10.1002/adma.201701218.
[196] Q. Chen, P.-F. Cao, R.C. Advincula, Adv. Funct. Mater. 28 (2018) 1800631, https://doi.org/10.1002/adfm.201800631.

Please cite this article in press as: X. Sui et al., Materials Today, (2021), https://doi.org/10.1016/j.mattod.2021.02.001

[197] T. Wu, E. Gray, B. Chen, J. Mater. Chem. C 6 (2018) 6200–6207, https://doi.org/10.1039/C8TC01092G.
[198] J.-Y. Choi et al., ECS J. Solid State Sci. Technol. 4 (2015) P3001–P3009, https://doi.org/10.1149/2.0011504jss.
[199] K. Chizari et al., Small 12 (2016) 6076–6082, https://doi.org/10.1002/smll.201601695.
[200] K. Fukuda et al., Nat. Commun. 5 (2014), https://doi.org/10.1038/ncomms5147.
[201] E.B. Secor et al., Adv. Electron. Mater. 4 (2018) 1700483, https://doi.org/10.1002/aelm.201700483.
[202] X. Pu et al., Sci. Adv. 3 (2017) e1700015, https://doi.org/10.1126/sciadv.1700015.
[203] Z. Deng et al., ACS Appl. Mater. Interfaces 11 (2019) 6796–6808, https://doi.org/10.1021/acsami.8b20178.
[204] W.J. Hyun, C.M. Thomas, M.C. Hersam, Adv. Energy Mater. (2020), https://doi.org/10.1002/aenm.202002135.
[205] W.J. Hyun et al., Faraday Discuss (2020), https://doi.org/10.1039/c9fd00113a.
[206] X. Kuang et al., Adv. Funct. Mater. 29 (2019), https://doi.org/10.1002/adfm.201805290.
[207] Z. Ding et al., Sci. Adv. 3 (2017) e1602890, https://doi.org/10.1126/sciadv.1602890.
[208] G. Liu et al., Sci. Adv. 4 (2018) eaat0641, https://doi.org/10.1126/sciadv.aat0641.
[209] V. Subramanian et al., Proc. IEEE 103 (2015) 567–582, https://doi.org/10.1109/JPROC.2015.2408321.

Please cite this article in press as: X. Sui et al., Materials Today, (2021), https://doi.org/10.1016/j.mattod.2021.02.001